

1 Zinc Phthalocyanine-Functionalized Polyvinyl  
2 Chloride Surfaces for Singlet Oxygen-Mediated  
3 Antibacterial and Antiviral Activity

4

5 *Hana Pistekova, <sup>1\*</sup> Martina Pummerova, <sup>1\*</sup> Monika Strasakova, <sup>1</sup> Miroslava Dusankova, <sup>1</sup>*

6 *Martin Novak, <sup>1</sup> Radka Korinková, <sup>2</sup> Vojtech Trousil, <sup>2</sup> Dominika Hanusova, <sup>1</sup> Jakub Sevcik, <sup>1</sup>*

7 *Eva Domincova Bergerova <sup>1</sup> and Vladimir Sedlarik <sup>1\*</sup>*

8

9

10 <sup>1</sup>Centre of Polymer Systems, University Institute, Tomas Bata University in Zlin, tr. Tomase  
11 Bati 5678,760 01 Zlin, Czech Republic

12 <sup>2</sup>Centre of Organic Chemistry ltd., CZ 533 54 Rybitvi 296, Czech Republic

13

14

15 \*Corresponding authors: Hana Pistekova, [pistekova@utb.cz](mailto:pistekova@utb.cz); Martina Pummerova,  
16 [pummerova@utb.cz](mailto:pummerova@utb.cz); Vladimir Sedlarik, [sedlarik@utb.cz](mailto:sedlarik@utb.cz)

17

18

19 **Keywords:** Polyvinyl chloride (PVC); Zinc phthalocyanine; Photodynamic antimicrobial materials;  
20 Singlet oxygen; Antimicrobial polymer surfaces; Zinc pyrithione;

## 21 **Abstract**

22 Functional polymer surfaces that combine antimicrobial activity with retained processability  
23 and material integrity are of growing interest for healthcare and high-contact applications.  
24 This study reports a photodynamically active polyvinyl chloride (PVC) system functionalized  
25 with a methacrylate-modified zinc phthalocyanine photosensitizer (ZnPTC-HEMA) and zinc  
26 pyrithione (ZPT), prepared by industrially relevant melt-processing a compression-molding  
27 methods. The resulting material platform was used to establish relationships between  
28 composition, structure, photoactivity, antimicrobial performance, and polymer stability.  
29 Quantitative analysis revealed efficient singlet oxygen generation even at low ZnPTC-HEMA  
30 loadings, with activity approaching saturation at higher concentrations. Under visible-light  
31 irradiation, the modified PVC surfaces exhibited pronounced antibacterial activity against  
32 *Staphylococcus aureus* and achieved more than a 5-log reduction of the enveloped  
33 bacteriophage  $\Phi 6$ , while the non-enveloped phage  $\Phi X174$  remained unaffected. The addition  
34 of ZPT broadened antibacterial efficacy, including under dark conditions. Morphological,  
35 spectroscopic, thermal, and mechanical analyses confirmed homogeneous additive  
36 incorporation, preservation of the PVC chemical structure, and retention of material integrity  
37 at low-to-moderate additive loadings. Migration studies further showed no detectable release  
38 of ZnPTC-HEMA after prolonged aqueous exposure. These results demonstrate that  
39 phthalocyanine-functionalized PVC provides a scalable platform for light-responsive  
40 antimicrobial polymer materials in which photoactive function can be introduced without  
41 compromising key processing and performance characteristics.

42

## 43 **1. Introduction**

44 Despite substantial advances in prevention and treatment, seasonal influenza remains a major  
45 public-health burden, accounting for nearly 30% of the infectious disease share in Europe,

46 while recurrent pandemics continue to underscore the vulnerability of modern societies to  
47 respiratory viral outbreaks.<sup>1,2</sup> Although influenza is generally less virulent than pandemic  
48 respiratory infections, it frequently predisposes patients to secondary bacterial pneumonia,  
49 most commonly caused by *Staphylococcus aureus*, *Streptococcus pneumoniae* and  
50 *Streptococcus pyogenes*, thereby substantially increasing morbidity and mortality.<sup>1,3</sup> In  
51 parallel, the recent coronavirus disease 2019 (COVID-19) pandemic, caused by severe acute  
52 respiratory syndrome coronavirus 2 (SARS-CoV-2), further highlighted the urgent need for  
53 material-based strategies capable of reducing pathogen transmission at surfaces and  
54 interfaces.<sup>4</sup> Consequently, the development of antiviral and antibacterial functional materials  
55 for healthcare and daily-use applications has become an important research priority.<sup>5</sup>

56 The use of polymers in medical devices has risen sharply in recent decades. However, their  
57 widespread use is accompanied by a persistent risk of bacterial colonization, leading to  
58 biofilm formation. This limitation is particularly relevant for indwelling and short-term  
59 devices, including endotracheal tubes, catheters, and other polymer-based components that  
60 can support the adhesion and proliferation of both Gram-positive and Gram-negative bacteria,  
61 such as *Pseudomonas aeruginosa* and *Staphylococcus aureus*.<sup>6</sup> Among these materials,  
62 polyvinyl chloride (PVC) remains one of the most extensively used polymers in healthcare  
63 because of its low cost, transparency, flexibility, and excellent processability. Its compatibility  
64 with industrial manufacturing techniques such as extrusion, thermoforming, and blow  
65 molding has secured its continued use in tubing, blood bags, catheters, and intravenous  
66 therapy containers. Thus, despite increasing interest in alternative polymers, PVC continues to  
67 offer highly relevant and industrially scalable platform for the development of advanced  
68 antimicrobial medical materials.<sup>6,7</sup>

69 A key limitation of PVC is its hydrophobic surface character, which promotes microbial  
70 adhesion and contributes to hospital-acquired infection risk. Addressing this drawback has

71 therefore become an important objective in polymer and interface engineering, with current  
72 strategies focusing on surface modification or incorporation of functional additives. Recent  
73 advances highlight the potential of inorganic nanoparticles including TiO<sub>2</sub>, ZnO, and gold, to  
74 impart robust antimicrobial properties, thereby reaffirming PVC's relevance as a platform for  
75 innovation in next-generation medical materials.<sup>6</sup> However, the search for alternative light-  
76 responsive additives with strong photoinduced antimicrobial activity, high stability, and  
77 compatibility with polymer processing remains ongoing.

78 Phthalocyanines (PTCs) represent a promising yet underexplored class of antimicrobial  
79 photoactive compounds for polymer applications. These aromatic compounds consist of four  
80 isoindoline units connected by azomethine bridges, with the ability to incorporate metal ions  
81 in their central cavity, which modulates their photoactivity.<sup>8</sup> PTCs are well known as  
82 photosensitizers because of their intense absorption in the near-infrared region (about 700  
83 nm), enabling deep penetration. They are also distinguished by their exceptional singlet  
84 oxygen generation efficiency even at low concentrations, remarkable photostability, and  
85 structural versatility that allows facile chemical modification.<sup>9,10</sup> The photophysical properties  
86 of PTCs are greatly influenced by the presence and nature of the central metal ion. Metals  
87 with doubly occupied orbitals (i.e., paired electrons) and diamagnetic ions (which are repelled  
88 by magnetic fields), such as Zn<sup>2+</sup>, Al<sup>3+</sup>, and Ga<sup>3+</sup>, provide PTC complexes with high triplet  
89 yields, long lifetimes, and associated strong photodynamic activity.<sup>11</sup> Zinc phthalocyanines  
90 (ZnPTC) in particular are among the most extensively studied derivatives because they  
91 combine favorable photodynamic properties with relatively accessible synthesis and structural  
92 tunability.<sup>12</sup>

93 Several reports support the antimicrobial potential of phthalocyanine-based system.  
94 Grammatikova et al. (2019) demonstrated strong antibacterial activity of cellulosic material

95 impregnated with ZnPTC,<sup>13</sup> while Efimov et al. (2024) reported significant antiviral  
96 photodynamic effect in textiles impregnated with LASU phthalocyanine.<sup>14</sup> Fang et al. (2026)  
97 further showed that hybrid fibrous membranes composed of zinc phthalocyanine-  
98 polycaprolactone/gelatin achieved 99% antibacterial efficacy against *E. coli* and *S. aureus*.<sup>15</sup>  
99 More broadly, PTCs have also been investigated as visible-light-active photocatalysts for self-  
100 cleaning and environmental decontamination applications.<sup>8,16</sup> Nevertheless, their integration  
101 into melt-processable commodity polymers, especially PVC, remains insufficiently explored,  
102 and studies that simultaneously address antimicrobial performance and the resulting effects on  
103 polymer properties are still scarce.

104

105 Evaluation of new antimicrobial materials increasingly require both antibacterial and antiviral  
106 assessment. However, experiments involving human pathogenic viruses are often expensive,  
107 technically demanding, and constrained by biosafety requirements. In this regard,  
108 bacteriophages offer practical and informative viral surrogates because they are safe to  
109 handle, readily propagated to high titers, and supported by established purification and  
110 quantification protocols. Importantly, selected bacteriophages share key structural and  
111 physicochemical characteristics with eukaryotic viruses, including morphology, envelope  
112 presence or absence, capsid dimensions, genome material and disinfectant resistance.<sup>17,18</sup>  
113 Serrano-Aroca (2022) identified bacteriophage  $\Phi 6$  as a suitable surrogate for SARS-CoV-2  
114 and other enveloped viruses, including influenza and Ebola,<sup>19</sup> and additional studies by Dey et  
115 al. (2021) and Franke et al. (2021) further support the use of phage  $\Phi 6$  as a safe model for  
116 highly pathogenic enveloped viruses in diverse biotechnological contexts.<sup>20-22</sup> By contrast,  
117 bacteriophage  $\Phi X174$  has been widely employed as a surrogate for non-enveloped viruses,  
118 including enteric viruses, hepatitis A virus and poliovirus, in the studies of airborne  
119 transmission, filtration, and water purification.<sup>18,23,24</sup> Guo et al. (2018) also used  $\Phi X174$  to

120 investigate plasma-assisted inactivation, highlighting the central role of singlet oxygen in viral  
121 inactivation pathways.<sup>25</sup>

122 On the basis of this framework, the present study employed two tailless phages in antiviral  
123 assays: the enveloped *Pseudomonas* phage  $\Phi 6$  (*Cystoviridae* family) as a surrogate for  
124 enveloped human viruses, and the non-enveloped coliphage  $\Phi X174$  (*Microviridae* family) as  
125 a model for non-enveloped viruses.<sup>18</sup> This study aimed to develop and comprehensively  
126 evaluate a PVC-based polymer system with light-activated antimicrobial functionality enabled  
127 by phthalocyanine incorporation. The material was assessed for antibacterial activity against  
128 representative Gram-positive and Gram-negative bacteria and for antiviral performance  
129 against  $\Phi 6$  and  $\Phi X174$  as model enveloped and non-enveloped viruses, respectively. In  
130 addition to antimicrobial efficacy, we examined the effect of the active additive on key  
131 material parameters relevant to practical implementation, including additive dispersion,  
132 migration resistance, thermal stability, and mechanical performance. Although antiviral  
133 polymers and bacteriophage-based antiviral testing have each been reported previously,<sup>4</sup> to the  
134 best of our knowledge, this is the first study to integrate a zinc phthalocyanine photosensitizer  
135 into a melt-processed PVC matrix and systematically relate singlet oxygen generation and  
136 antimicrobial performance to polymer morphology, stability, and mechanical behavior.

137

## 138 **2. Materials and Methods**

### 139 **2.1 Materials**

140 PVC RB3 polymer matrix was purchased from ModenPlast Medical Srl (Ubersetto di Fiorino,  
141 Italy). The zinc 2-[3-(phthalocyaninesulphonamido)propoxy]ethylmetacrylate (ZnPTC-  
142 HEMA) was synthesized in the Centre of Organic Chemistry (Rybitví, Czech Republic). Zinc  
143 Pyrithione (ZPT) was supported by Alchimica (Prague, Czech Republic). All other chemicals  
144 were purchased from Merck (Prague, Czech Republic).

145

#### 146 **Preparation of ZnPTC-HEMA**

147 ZnPTC-HEMA was prepared by a three-step process (Figure 1). To begin, 304 mL of  
148 chlorosulphonic acid was placed in a 1.5 L flask and cooled to 0 – 5 °C in an ice bath. Then,  
149 100 g (173 mmol) of ZnPTC was added in portions, allowing the temperature to rise to 20 °C.  
150 The mixture was stirred at this temperature for 30 minutes, then heated to 120 °C for 1 hour.  
151 After cooling to 100 °C, 64 mL of thionyl chloride (SOCl<sub>2</sub>) was added dropwise, and the  
152 mixture was maintained at 100 °C for an additional hour. The reaction mixture was then  
153 cooled to 20 °C and poured onto a water-ice mixture. The resulting precipitate was collected  
154 by filtration, and the filter cake was washed repeatedly with cold water until no sulfate or  
155 chloride ions were detected. The resulting paste of phthalocyanine sulfochloride (Pc-SO<sub>2</sub>Cl,  
156 603 g) was stored in a refrigerator.

157 The paste was analyzed for hydrolyzable chlorine and dry matter content (dried at 80 °C). The  
158 dry matter was found to be 20.3%, and the hydrolyzable chlorine content (calculated based on  
159 dry mass) was 8.9% (the theoretical value for the bis-substituted derivative is 9.14%).

160 Next, 593 g of the frozen Pc-SO<sub>2</sub>Cl was thoroughly dispersed in 543 mL of cold water,  
161 followed by the addition of 39 mL of allylamine (521 mmol). The reaction mixture was  
162 heated to 40 °C and stirred for 5 hours, then cooled to room temperature and filtered. The  
163 filter cake was washed thoroughly with water to remove excess amine and dried at 50 °C,  
164 yielding 100 g (80%) of blue ZnPTC-AA.

165 Subsequently, 100 g of ZnPTC-AA was vigorously dispersed in 450 mL of cold water.  
166 Hydroxyethyl methacrylate (19.8 mL, 163 mmol) was then added under stirring. The pH of  
167 the reaction mixture (~7) was adjusted to 11 using 4 M NaOH, after which it was heated at  
168 60 °C for 1.5 hours. The mixture was cooled to approximately 25 °C and filtered. The filter

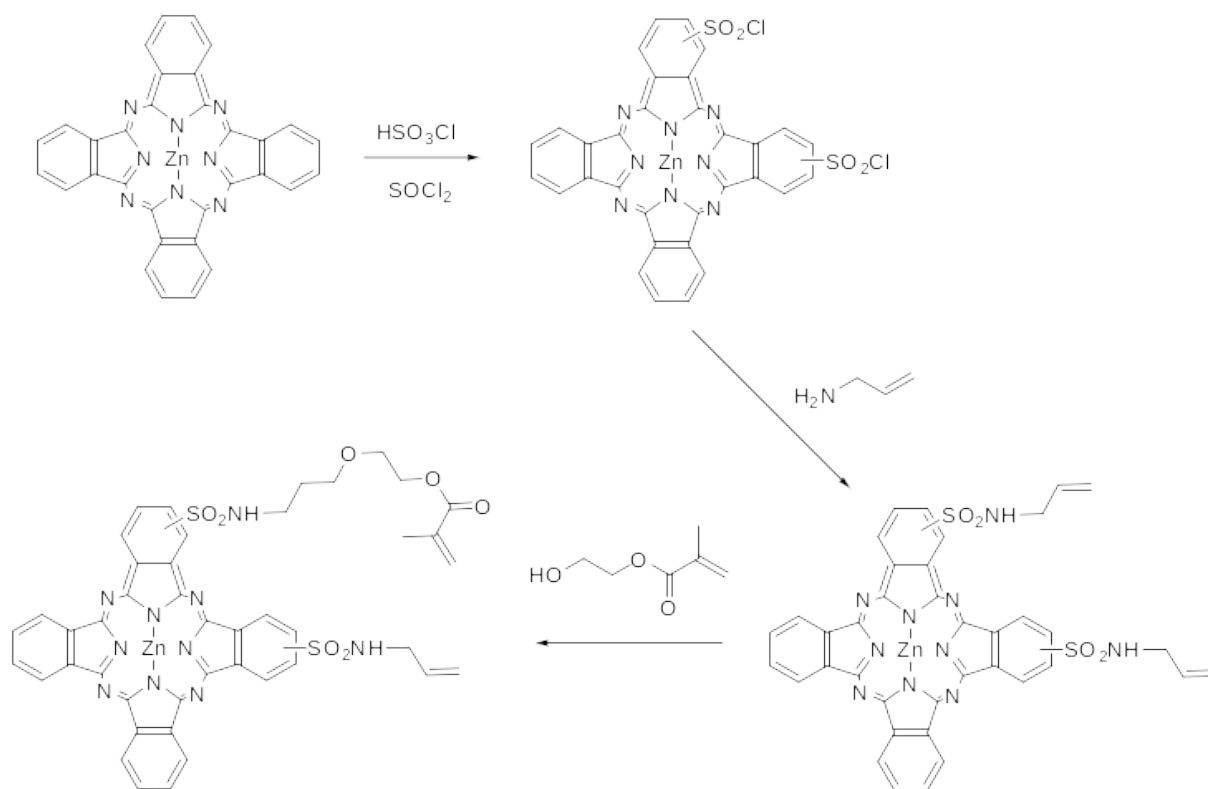
169 cake was washed with 100 mL of water and dried at 50 °C to afford 92 g (76%) of blue  
170 ZnPTC-HEMA.

171 <sup>1</sup>H and <sup>13</sup>C NMR spectroscopy of the final product was performed in DMSO. The spectra  
172 were complex due to the presence of multiple isomers with varying degrees of substitution.  
173 Nevertheless, several characteristic signals confirmed the molecular structure. In the <sup>1</sup>H NMR  
174 spectrum, two distinct signals corresponding to the methylene group were observed at 5.7 and  
175 6.3 ppm, along with a singlet at 11.0 ppm for the NH group and a methyl signal at 1.9 ppm.  
176 The <sup>13</sup>C NMR spectrum confirmed the presence of the ester carbon of the methacrylate group  
177 at 166.7 ppm, as well as eight aliphatic carbon signals, including the terminal methyl at 18.0  
178 ppm.

179 2,5-Bis(2-ethylhexyl)-3,6-diphenyl-1H,2H,4H,5H-pyrrolo[3,4-c]pyrrole-1,4-dione (DPP) was  
180 synthesized following a modified procedure based on Pop et al. (2019), in which K<sub>2</sub>CO<sub>3</sub>/DMF  
181 was employed instead of Cs<sub>2</sub>CO<sub>3</sub>/CH<sub>3</sub>CN.<sup>26</sup>

182 3,6-Diphenyl-1,4-diketopyrrolo[3,4-c]pyrrole (5.00 g, 17.34 mmol) was suspended in  
183 anhydrous DMF (150 mL) under a nitrogen atmosphere. Finely powdered K<sub>2</sub>CO<sub>3</sub> (9.60 g,  
184 69.37 mmol) was added, and the resulting heterogeneous mixture was stirred at 125 °C for 1  
185 h. 2-Ethylhexyl bromide (13.4 g, 69.37 mmol) was then added dropwise over 3 h, and the  
186 reaction mixture was maintained at 125 °C for an additional 20 h.

187 After cooling to room temperature, the reaction mixture was poured into excess water to  
188 induce precipitation. The resulting solid was collected by vacuum filtration, washed  
189 thoroughly with water, and dried under reduced pressure. Purification by recrystallization  
190 from hot methanol afforded the target compound as a red solid (1.6 g, 18% yield).



191

192 **Figure 1.** Synthetic route yielding ZnPc-HEMA.

193

#### 194 **Sample preparation**

195 Firstly, the PVC compound RB3 polymer masterbatch, plasticized with di-2-ethylhexyl  
 196 phthalate (DEHP) and ZPT, was processed using a Brabender Plastograph (Brabender GmbH  
 197 & Co. KG, Duisburg, Germany) at 50 RPM for 3 minutes at 150 °C and then set aside for  
 198 further steps. Secondly, the PVC mixture with the ZnPTC-HEMA additive was melt-  
 199 compounded under identical conditions for 6 minutes to achieve a homogenized blend.

200 A calculated amount of this masterbatch and the PVC-ZnPTC-HEMA blend were then  
 201 reprocessed using an Xplore MC15 micro-compounder (Xplore Instruments BV, Sittard, The  
 202 Netherlands) at 150 °C and 100 RPM for 5 minutes. The final composition of the samples is  
 203 listed in Table 1. For comparison, a reference PVC sample was prepared under the same  
 204 conditions and with the same instruments.

205 The final processing step involved compression moulding with a FONTIJNE LabEcon 300  
 206 hydraulic press (Fontijne Presses b.v., Rotterdam, The Netherlands) at 150 °C, with an 8-  
 207 minute tempering period, followed by 3 minutes of pressing at 200 kN and 3 minutes of  
 208 cooling at 400 kN using a Metallkraft WPP 50 M press (Stürmer Maschinen GmbH,  
 209 Hallstadt, Germany).

210

211 **Table 1.** Quantification of singlet oxygen with varying concentrations of ZnPTC-HEMA

Sample name	Component (wt %)		
	PVC	ZnPTC-HEMA	ZPT
PVC-0	100	-	-
PVC-0.1	99.9	0.1	-
PVC-0.2	99.8	0.2	-
PVC-0.5	99.5	0.5	-
PVC-1	99.0	1.0	-
PVC-3	97.0	3.0	-
PVC-0-ZPT	100	-	0.005
PVC-0.1-ZPT	99.9	0.1	0.005
PVC-0.2-ZPT	99.8	0.2	0.005
PVC-0.5-ZPT	99.5	0.5	0.005
PVC-1-ZPT	99.0	1.0	0.005
PVC-3-ZPT	97.0	3.0	0.005

212

## 213 2.2 Morphology analysis

214 FEI NanoSEM 450 (FEI Company, The Netherlands) was used to analyse the morphology of  
 215 PVC samples' fracture in order to evaluate the degree of homogeneity. The microscope was

216 operated in vacuum mode at an acceleration volage of 5 kV. The samples were beforehand  
217 sputtered with gold and palladium for 30 s.

218

### 219 **2.3 Chemical structure analysis - Fourier transform infrared spectroscopy (ATR-FTIR)**

220 Infrared spectra were recorded using a Nicolet iS5 FTIR spectrometer (Thermo Fisher  
221 Scientific, USA) equipped with a diamond ATR crystal. Spectra were collected over the range  
222 4000–400  $\text{cm}^{-1}$  at a resolution of 4  $\text{cm}^{-1}$ , averaging 64 scans per sample.

223

### 224 **2.4 Colorimetric analysis**

225 The colorimetric properties of the PVC samples were analyzed using a UltraScan VIS  
226 spectrophotometer (Hunter Lab, USA). The primary analysis utilized the D65/10° spectrum,  
227 which simulates daylight at 6500 K, with a viewing angle consistent with the D/8 geometry of  
228 the HunterLab Ultrascan instrument.

229

### 230 **2.5 Thermal properties**

231 The thermal stability and thus the suitability of additives for thermoplastic processing were  
232 confirmed using thermogravimetric analysis (TGA). Samples for thermogravimetry  
233 measurement were prepared at 8 mg in weight and investigated on a TA Q500  
234 thermogravimetric analyser (TA Instruments, Wilmington, DE, USA) by a TA Universal  
235 Analyzer 2000 version 4.5A (TA Instruments – Waters LLC, Wilmington, DE, USA). The  
236 instrument was set to a heating rate of 10  $^{\circ}\text{C}/\text{min}$  from 25 to 800  $^{\circ}\text{C}$  under a nitrogen  
237 atmosphere. Data of initial degradation temperature ( $T_i$ ), the peak degradation temperature  
238 with maximum weight loss rate ( $T_p$ ), and thermal degradation weight loss of both  
239 antimicrobials were collected.

## 240 **2.6 Singlet Oxygen Quantification**

241 Singlet oxygen production generation was quantified using the 1,3-diphenylisobenzofuran  
242 (DPIBF) method in hexan. DPIBF selectively reacts with intermediate singlet oxygen  $^1\text{O}_2$  to  
243 form an unstable peroxide that decomposes into the colourless product 1,2-dibenzoylbenzene,  
244 enabling specific detection without interference from other reactive oxygen species. Hexane  
245 was selected as the solvent because it dissolves DPIBF while leaving PVC and ZnPTC-  
246 HEMA insoluble, and it provides a higher molar oxygen solubility compared to water.

247 Polymer samples were cut into  $8 \times 8$  mm squares, accurately weighed, and placed at the  
248 bottom of a spectrophotometer cuvette. Subsequently, 2 mL of hexane and DPIBF ( $c \approx 2$  g/L)  
249 were added to reach absorbance  $\lambda = 417$  nm in the range 0.7–0.8. The samples were irradiated  
250 with a 661 nm laser (40 mW, focused beam), and the decrease in absorbance at 417 nm was  
251 monitored to follow the reaction kinetics. The rate constant  $k$  ( $\text{J}^{-1}$ ), proportional to  $^1\text{O}_2$   
252 generation, was determined from the absorbance decay as a function of incident light energy.  
253 From these slopes, the indicator half-life values ( $\tau_{1/2}$ , s) were calculated for each sample.<sup>27</sup>

## 254 **2.7 Antimicrobial assays**

### 255 **Antibacterial efficacy**

256 The antibacterial efficacy of the investigated samples was evaluated under laboratory  
257 conditions using standardized test microorganisms and procedures, as detailed below. Before  
258 antibacterial testing, samples and polypropylene foils were disinfected by rinsing with 70%  
259 denatured ethanol. For the determination two bacterial strains were used, Gram-negative  
260 *Escherichia coli* CCM 4517 and Gram-positive *Staphylococcus aureus* CCM 4516 purchased  
261 from the Czech Collection of Microorganisms (Brno, Czech Republic). These bacteria were  
262 selected as model microorganisms because they represent environmentally relevant species.  
263 The antibacterial testing was performed according to ISO 22196 with modifications. Bacterial  
264 suspensions (*Escherichia coli*  $3,4 \cdot 10^5$  CFU/mL; *Staphylococcus aureus*  $1,2 \cdot 10^5$  CFU/mL) were

265 prepared in 500x diluted Nutrient broth (HiMedia laboratories, India). The bacterial  
266 suspension was dispensed on the sample surface (dimensions 25×25 mm) in the volume  
267 100 µL and the sample was covered with the polypropylene foil (dimensions 20×20 mm).  
268 Samples with foils were cultivated at 35 °C and ≥90% relative humidity for 18 hours. The  
269 samples for illumination were incubated in a polymethylmethacrylate incubator with  
270 transparent walls and illuminated from a distance of 200 cm by an artificial daylight source  
271 (LED source: blue primary emitter 450 nm; Illumination intensity = 1250 lx). After the  
272 incubation time, polypropylene foil was removed and each sample was completely washed by  
273 SCDLP broth (HiMedia laboratories, India), which was subsequently collected. The viable  
274 bacteria count was determined by the pour plate culture method (PCA, HiMedia laboratories,  
275 India). After the incubation, the number of bacteria colonies in the Petri dishes was  
276 determined.

277 The antibacterial activity (R) was calculated using Equation (1):

278

$$279 \quad R = \log N_{\text{blank}} - \log N_{\text{sample}}, \quad (1)$$

281 where  $\log N_{\text{blank}}$  and  $\log N_{\text{sample}}$  are the logarithms of viable bacteria number in the reference  
282 and modified sample, respectively. All experiments were conducted in triplicate, with  
283 a minimum of two independent determinations for each parameter.

284 Statistical significance was evaluated by applying one-way ANOVA ( $P < 0.05$ ); (OriginPro  
285 2024, OriginLab Corporation, Massachusetts, USA); experimental data are reported as the  
286 mean values of three replicates  $\pm$  standard deviation.

287

### 288 **Antiviral efficacy**

289 In this work, bacteriophages *Pseudomonas* phage  $\Phi 6$  DSM 21518, *Escherichia* phage  $\Phi X174$   
290 DSM 4497 and their host cultures *Pseudomonas syringae* DSM 21518 and *Escherichia*

291 *coli* DSM 13127 were sourced from Leibniz Institute DSMZ-German collection of  
292 Microorganisms and Cell Culture GmbH (Braunschweig, Germany). The received  
293 microorganisms were cultured following the manufacturer's instructions. Stock cultures of *P.*  
294 *syringae* and *E. coli* were stored at -70°C, whilst the  $\Phi 6$  and  $\Phi X174$  bacteriophages were  
295 stored in refrigerator at 4°C.

296 The antiviral activity of the samples was compared to neat PVC without active substances in a  
297 polymer matrix and were performed according to a modified ISO 22196:2021 standard.  
298 A phage lysate with an initial viral particle concentration of approximately  $10^9$  PFU/mL,  
299 prepared according to the supplier's instructions, was diluted 500-fold in nutrient broth  
300 (HiMedia Laboratories, India) to obtain viral suspensions with final concentrations of  $\Phi 6$  ( $1.8$   
301  $\times 10^6$  PFU/mL) and  $\Phi X174$  ( $7.7 \times 10^6$  PFU/mL). Samples were incubated with the respective  
302 viral suspensions for 18 h. Incubation was carried out according to the preferences of the host  
303 culture: 25 °C for phage  $\Phi 6$  and 35 °C for  $\Phi X174$  and relative humidity  $\geq 90\%$ . After rinsing  
304 the samples, phage was assayed by the double layer method, when phage suspension (0.1 mL)  
305 was mixed with 0.1 mL host culture (OD = 0.3) and 3 mL top agar and poured on to surface  
306 of a bottom agar plate. Sterilization of the samples, methodology, sample dimensions and  
307 calculation of antiviral activity were the same as for bacteria.

308

## 309 **2.8 Migration study**

310 Migration testing was carried out according to ČSN EN 1186 (Migration from plastics into  
311 food simulants). Prior to testing, PVC foils containing phthalocyanines were rinsed with  
312 demineralized water and dried on filter paper. Samples were immersed in distilled water,  
313 maintaining a contact ratio of 1 dm<sup>2</sup>/100 mL. Incubation was performed at 40 °C for 10 days  
314 (240 h) in the dark with mild agitation (110 rpm), representing standard migration conditions  
315 for long-term room temperature contact. Control samples (pure water and PVC without

316 phthalocyanine) were prepared in parallel. The same prepared samples were also subjected to  
317 UV-Vis and EDX-XRF analysis, respectively.

318

### 319 **UV-Vis analysis**

320 Measurements were carried out on a Tecan Infinite 200 PRO (Tecan, Austria). Absorption  
321 spectra of the calibration series (0.01–5.0 µg/mL) were recorded in the range of 300–800 nm.  
322 The absorption maximum was determined at 628 nm, which was subsequently used for  
323 quantitative measurements. The limit of detection for this method was 0.24 µg of PTC per  
324 mL.

325

### 326 **EDX-XRF analysis**

327 The content of elements in the sample water extracts was determined by EDX-XRF method  
328 (Energy ray dispersion spectroscopy - X ray fluorescence), which is based on elemental  
329 analysis of X-ray diffraction (energy) materials. The amount of element analyzed was  
330 evaluated in weight percent (wt %).

331 Samples in special cups were placed (3 g) inside the instrument at the appropriate sample to  
332 autosampler. The content of the elements was determined using an Energy Dispersive X-ray  
333 Spectrometer (Thermo Scientific, ARL Quant X). The samples were analyzed in a special  
334 selected method: Any sample Air in Quant Unite program. The limit of detection is until: 0.1  
335 – 0.5 wt %, and the limit of quantification is until: 0,1 wt %.

336

## 337 **3. Results and Discussion**

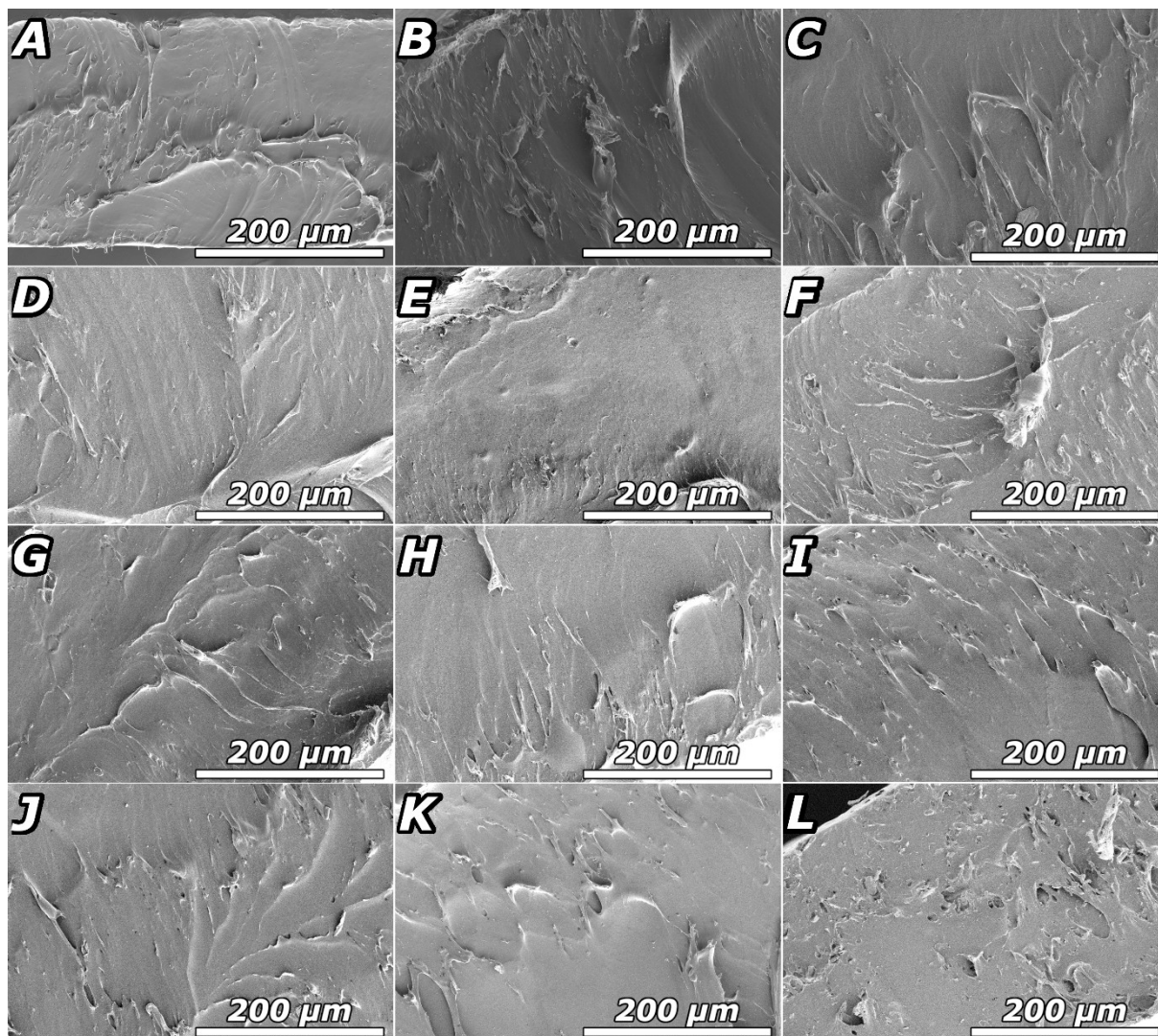
### 338 **3.1 Morphology analysis**

339 The morphology of the prepared PVC samples was investigated by SEM. Representative  
340 surface micrographs of cryo-sectioned moulded foils are shown in Figure 2. Discrete

341 particulate features were observed within a narrow size range across all samples, including  
342 neat PVC (Figure 2A), despite the absence of intentionally added additives. Their ubiquitous  
343 presence strongly suggests that these particulates originate from processing additives  
344 incorporated by the PVC granulate manufacturer to enhance material performance, as  
345 previously reported.<sup>28,29</sup>

346 In comparison with neat PVC (Figure 2A), the PVC sample containing ZPT (0.005 wt %;  
347 Figure 3G) exhibits a homogeneous morphology with no discernible ZPT particles, indicating  
348 good compatibility and dispersion of ZPT within the PVC matrix. Similarly, samples  
349 containing Zn-PTC-HEMA at lower loadings (Figure 2B–E and Figure 2H–K) display  
350 smooth fracture surfaces and a uniform distribution of PTC, with no evidence of particle  
351 agglomeration.

352 In contrast, samples containing 3 wt % Zn-PTC-HEMA, both without and with ZPT (Figure  
353 2F and Figure 2L, respectively), show a homogeneous matrix populated by a markedly higher  
354 number of particulate features. Notably, sample L exhibits a significantly roughened fracture  
355 surface. This morphology is indicative of an excessive loading of the phthalocyanine additive,  
356 leading to microstructural heterogeneity. The observed surface roughness correlates well with  
357 the deterioration in mechanical properties discussed in the following section. Similar effects  
358 associated with high PTCs loadings in polymer matrices have been reported elsewhere.<sup>30</sup>



359

360 **Figure 2.** SEM images of A) PVC-0, B) PVC-0.1, C) PVC-0.2, D) PVC-0.5, E) PVC-1, F)  
 361 PVC-3, G) PVC-0-ZPT, H) PVC-0.1-ZPT, I) PVC-0.2-ZPT, J) PVC-0.5-ZPT, K) PVC-1-ZPT,  
 362 L) PVC- 3-ZPT.

363

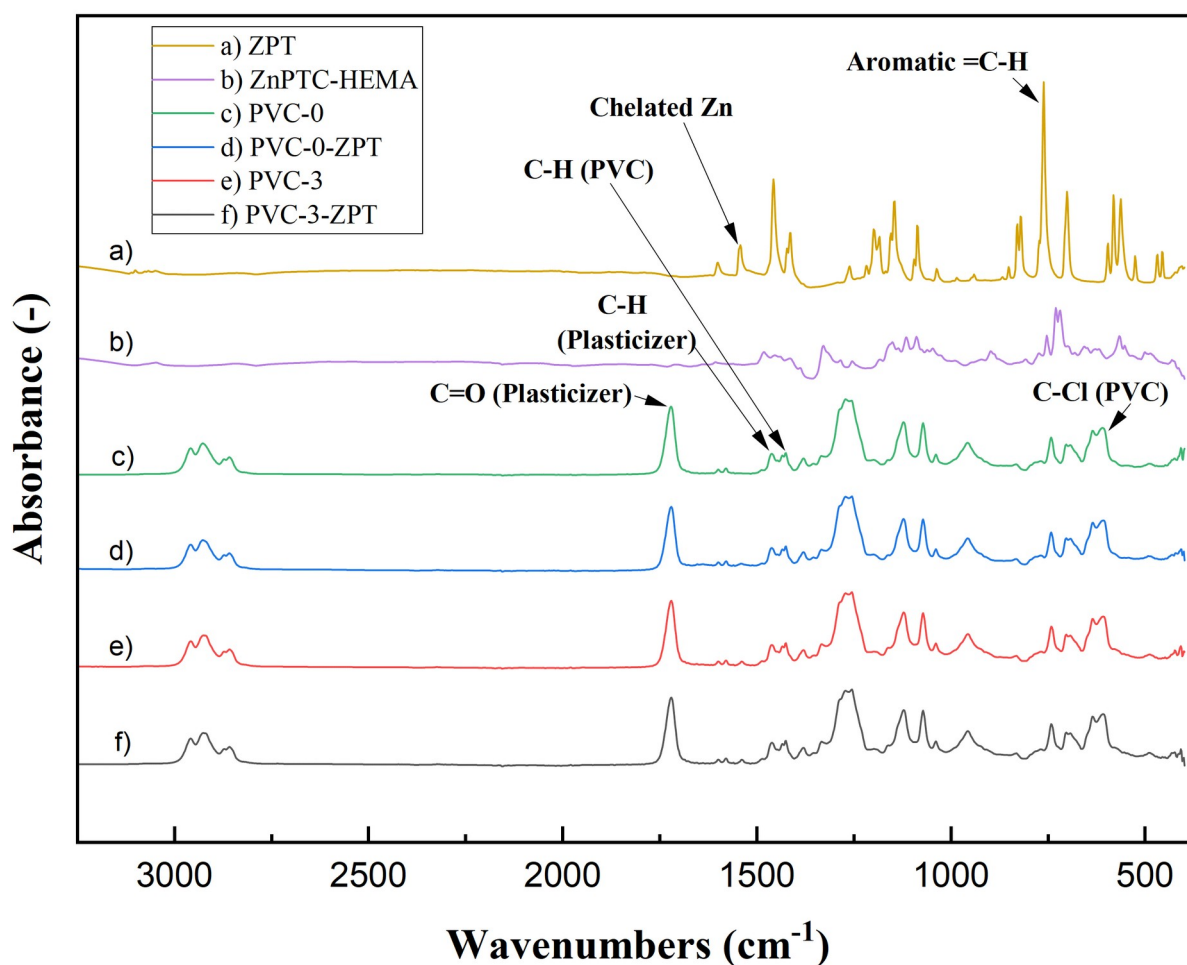
### 364 3.1 Chemical structure analysis - Fourier transform infrared spectroscopy (ATR-FTIR)

365 The FTIR spectrum of neat PVC exhibits characteristic absorption bands associated with  
 366 specific functional groups in the repeating  $-\text{CH}_2-\text{CHCl}-$  units (Figure 3). Strong bands at  
 367  $2970-2850\text{ cm}^{-1}$  correspond to C-H stretching vibrations of the methylene ( $-\text{CH}_2-$ ) groups,  
 368 typical of aliphatic polymers and indicative of the saturated polymer backbone. The  
 369 prominent band at  $1425\text{ cm}^{-1}$  arises from  $\text{CH}_2$  scissoring vibrations and is a key diagnostic

370 feature of PVC. Additional bands in the 1330–1250  $\text{cm}^{-1}$  region are assigned to  $\text{CH}_2$  wagging  
371 and rocking modes, while those at 1095–1020  $\text{cm}^{-1}$  correspond to C–C stretching vibrations  
372 along the polymer chain. A distinctive set of absorptions between 960 and 610  $\text{cm}^{-1}$  is  
373 attributed to C–Cl stretching vibrations, which are characteristic of PVC and confirm the  
374 presence of chlorine in the macromolecular structure.

375 Bands near 1730  $\text{cm}^{-1}$  (C=O stretching) and 1650  $\text{cm}^{-1}$  (C=C stretching), which would  
376 indicate oxidation or dehydrochlorination, are absent, confirming that the material is  
377 chemically unaltered PVC. Overall, the obtained FTIR spectrum agrees well with reference  
378 data<sup>31,32</sup> and displays all diagnostic features of unmodified PVC, including pronounced C–H,  
379  $\text{CH}_2$ , and C–Cl absorptions. The FTIR spectra of PVC formulations containing additives  
380 closely resemble that of neat PVC (PVC-0). However, a distinct weak band at  $\sim 1538 \text{ cm}^{-1}$   
381 appears exclusively in the modified samples and is absent in neat PVC. This band is attributed  
382 to coordination-sensitive ring vibrations of ZPT and confirms its successful incorporation in  
383 the polymer matrix. Its position ( $\approx 1536\text{--}1538 \text{ cm}^{-1}$ ) corresponds to ligand ring vibrations  
384 sensitive to metal coordination, supporting the presence of Zn–pyrithione in a chelated form.<sup>33</sup>

385 FTIR spectroscopy shows that, even at the highest loadings of ZnPTC-HEMA and ZPT, the  
386 characteristic bands of PVC remain unchanged in position and relative intensity (Figure 3).  
387 This indicates that incorporation of these additives does not alter the chemical environment of  
388 the PVC chains, implying the absence of chain rearrangement, disruption of the polymer  
389 backbone, or formation of new interactions that would modify the matrix structure.



390

391

392 **Figure 3.** FTIR spectra for pure ZnPTC-HEMA; a) pure ZPT, b) ZnPTC-HEMA, c) PVC-0,  
 393 d) PVC-0-ZPT, e) PVC- 3 and f) PVC- 3-ZPT. In accordance with Deleanu et al. (2024).<sup>34</sup>

394

### 395 3.2 Colorimetric study

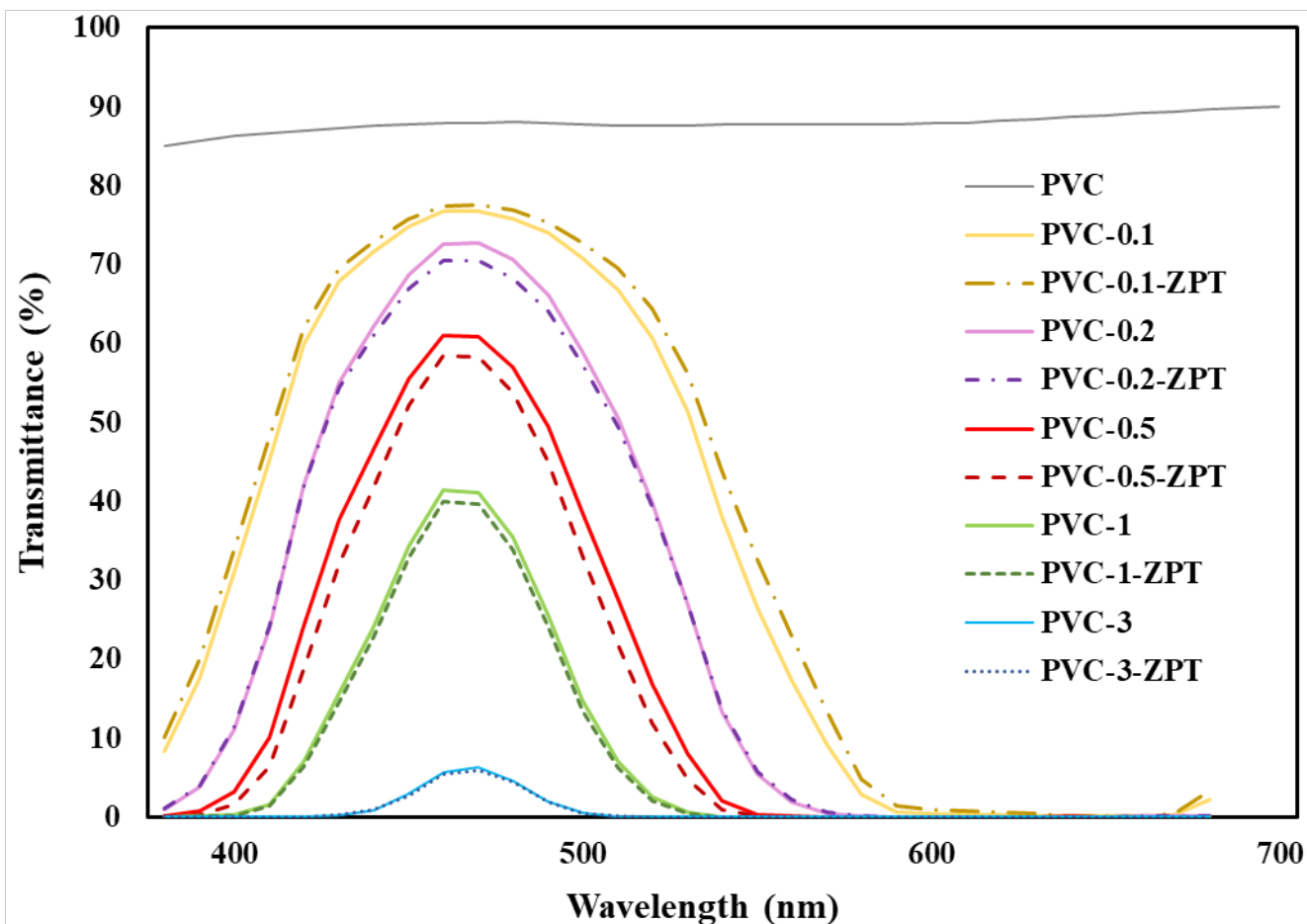
396 The transmission spectra (Figure 4) of neat PVC (PVC-0) and PVC compounds containing  
 397 ZnPTC-HEMA at different loadings (0.1–3.0 wt %), with and without the presence of ZPT  
 398 (0.005 wt %), reveal distinct modifications in optical behavior that are strongly dependent on  
 399 the concentration of ZnPTC-HEMA (Figure 4).

400 Neat PVC exhibits a baseline spectrum typical of an unmodified polymer matrix, with  
 401 relatively high transmission across the visible region and minimal absorption features.<sup>35</sup> Upon

402 incorporation of **ZnPTC-HEMA at low concentrations (0.1–0.2 wt %)**, a slight decrease in  
403 transmission is observed, indicating the introduction of weak absorptive species into the  
404 polymer matrix. The effect is slightly more pronounced with the simultaneous introduction of  
405 ZPT.

406 At concentrations of 0.5–1.0 wt % ZnPTC-HEMA, the spectra reveal a pronounced reduction  
407 in transmittance, most notably within the UV region. This trend is attributable to the increased  
408 absorbance associated with the higher density of ZnPTC-HEMA chromophore units. Co-  
409 addition of ZPT induces a further, albeit modest, decrease in transmittance; however, the  
410 relative influence of ZPT diminishes progressively with increasing ZnPTC-HEMA  
411 concentration.

412 At the highest concentration examined (3.0 wt % ZnPTC-HEMA; samples PVC-3 and PVC-  
413 3-ZPT), the spectra exhibit the lowest overall transmittance, characterized by substantial  
414 attenuation across both the UV and visible regions. Under these conditions, the presence of  
415 ZPT does not produce a significant additional suppression of transmittance, indicating that  
416 optical shielding is dominated by the ZnPTC-HEMA component at this concentration.



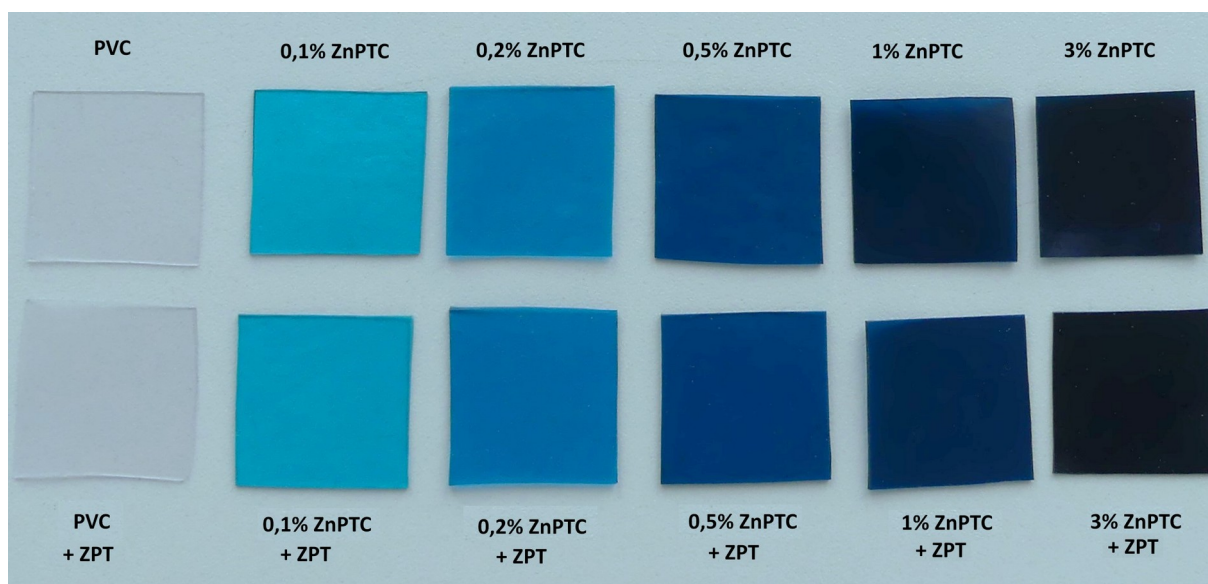
417

418

419 **Figure 4.** Transmission spectra of PVC-0; PVC-0.1; PVC-0.1- ZPT; PVC-0.2; PVC-0.2-ZPT;  
 420 PVC-0.5; PVC-0.5-ZPT; PVC-1; PVC-1-ZPT; PVC-3; PVC-3-ZPT.

421

422 The visual appearance of the samples (Figure 5) is fully consistent with the spectroscopic  
 423 data. Increasing ZnPTC-HEMA concentration leads to a progressive darkening and loss of  
 424 transparency, while samples with and without ZPT at the same ZnPTC-HEMA loading are  
 425 visually indistinguishable or show only negligible differences. Together, these results  
 426 demonstrate that the colorimetric and optical properties of the compounds are controlled  
 427 almost exclusively by ZnPTC-HEMA content. The addition of ZPT at 0.005 wt % does not  
 428 significantly affect the transmission behavior, confirming that ZPT can be incorporated  
 429 without compromising the optical characteristics of the PVC/ZnPTC-HEMA compound.



430

431 **Figure 5.** PVC samples with increasing ZnPTC-HEMA; PVC-0, PVC-0.1, PVC-0.2, PVC-  
 432 0.5, PVC-1, PVC-3; (top) and with the addition of ZPT (0.005 wt %); PVC-0.1-ZPT, PVC-  
 433 0.2-ZPT, PVC-0.5-ZPT, PVC-1-ZPT, PVC- 3-ZPT (bottom).

434

### 435 3.2 Thermal properties

436 The applicability of antimicrobial agents incorporated into polymers is determined not only  
 437 by their compatibility with the polymer matrix but also by their thermal stability. PVC  
 438 undergoes thermal degradation in distinct stages. The initial degradation phase occurs  
 439 between 25 °C and 350 °C and is primarily associated with dehydrochlorination and the  
 440 volatilization of plasticizers, such as di(2-ethylhexyl) phthalate (DEHP).<sup>36</sup> This stage  
 441 exhibited two distinct degradation events, with peak maxima at 255 °C and 280 °C. During  
 442 this phase, a weight loss of approximately 72.4 wt % was observed, with the maximum  
 443 degradation rate occurring at 280 °C (Table 2), as indicated by the peak temperature (Tp) on  
 444 the DTG curve. This is in accordance with other studies of thermal behavior of PVC.<sup>37,38</sup>

445 The second degradation stage occurred between 350 °C and 600 °C and is likely associated  
 446 with the breakdown of conjugated polyenes into benzene and alkylated benzenes, as well as  
 447 the thermal cracking of the polymer backbone. Finally, at temperatures above 600 °C, the last

448 degradation stage takes place, which can be attributed to the decomposition of byproducts,  
 449 such as hydrocarbon residues, formed during the earlier degradation processes.<sup>38-40</sup>  
 450 The incorporation of the antimicrobial agents ZPT and ZnPTC-HEMA had only a minor  
 451 effect on the thermal degradation behavior of PVC. Unlike neat PVC (PVC-0), the compound  
 452 material (PVC-3-ZPT) exhibited a single broad degradation step in the temperature range of  
 453 25 °C to 350 °C, with a peak maximum at 280 °C, which is characteristic of PVC with no  
 454 significant difference in weight loss. The influence of the antimicrobial agents became more  
 455 apparent in the subsequent degradation stages. Although these stages occurred within the  
 456 same temperature ranges as for neat PVC, they exhibited varying weight changes.  
 457 Specifically, the second degradation step showed reduced weight loss in the presence of ZPT,  
 458 while the addition of ZnPTC-HEMA resulted in increased weight loss during the final  
 459 degradation stage. To support these observations, TGA of the pure antimicrobial agents was  
 460 also conducted to better understand their individual thermal degradation behaviors. Overall,  
 461 the total weight loss was approximately 92.41 wt % for neat PVC (PVC-0) and 88.41 wt % for  
 462 the PVC/ZPT/ZnPTC-HEMA compound (PVC-3-ZPT).

463

464 **Table 2.** Thermal characterization analysis of antimicrobial additives and PVC

Samples	T <sub>i</sub> (°C)	T <sub>p</sub> (°C)	Temperature range (°C)		
			Weight loss (wt %)		
			25-350	350-600	600-800
PVC-0	197	280	72.38	19.23	0.80
PVC- 3-ZPT	200	278	71.11	15.81	1.49
			25-150	150-420	420-800
ZnPTC-HEMA		322	3.70	23.07	37.2
			25-420	420-600	600-800

ZPT	265	282	49.04	5.53	5.31
-----	-----	-----	-------	------	------

465 *the initial decomposition (onset) temperature ( $T_i$ ), the peak maximum on DTG curve  $T_p$*

466

467 For the pure ZPT, the degradation initiation temperature was observed at approximately  
 468 265 °C, with the first peak maximum occurring at 282 °C (Table 2). The overall thermal  
 469 decomposition can be divided into three distinct degradation stages. The first stage, associated  
 470 with the decomposition of the ZPT complex, occurred within the temperature range of 25 °C  
 471 to 420 °C. This stage exhibited two distinct degradation events, with peak maxima at 282 °C  
 472 and 330 °C, which are consistent with values reported in the literature.<sup>41</sup> These peaks are  
 473 attributed to the solid-state dimeric structure of ZPT.

474 The second degradation stage, characterized by a weight loss of 5.53 wt %, occurred between  
 475 420 °C and 600 °C and is likely associated with the degradation of specific components of the  
 476 ZPT complex. The final degradation stage, observed at temperatures above 600 °C, is  
 477 attributed to the decomposition of residual byproducts.

478 Additionally, ZPT exhibits a melting point of approximately 240 °C, which facilitates its  
 479 incorporation into a range of thermoplastics and elastomers. Notably, previous studies have  
 480 shown that the addition of ZPT does not compromise the thermal stability of high-density  
 481 polyethylene (HDPE) foils, indicating that ZPT can be effectively used in polymer matrices  
 482 without significantly affecting their thermal properties.<sup>42</sup>

483 The thermal stability of the pure ZnPTC-HEMA dye was also evaluated using the TGA. The  
 484 TGA curve revealed multiple decomposition steps. The initial weight loss of 3.70 wt % was  
 485 observed from room temperature up to 150 °C (Table 2), corresponding to the evaporation of  
 486 adsorbed moisture.

487 The degradation behavior of this newly synthesized material was complex and analyzed  
 488 in terms of the decomposition of its constituent components. Specifically, the PTC segment

489 degraded in two distinct temperature intervals, with degradation of the HEMA component  
490 occurring between these stages. The soft HEMA segments degraded in the temperature range  
491 of 200 °C to 420 °C, with a maximum degradation rate at 322 °C. Additionally, the initial  
492 degradation of the PTC component began earlier, between 150 °C and 200 °C, and was  
493 attributed to the breakdown of the phthalocyanine ring.

494 At elevated temperatures above 420 °C, the degradation of both the PTC component and the  
495 hard HEMA segments continued, with overlapping processes that prevented the clear  
496 distinction of individual degradation steps. For instance, the hard HEMA segments were  
497 expected to degrade within the range of 327 °C to 670 °C, while the residual PTC component  
498 decomposed between 450 °C and 700 °C. Despite the complexity, the overall decomposition  
499 behavior observed in this study is consistent with previously reported findings.<sup>43-45</sup>

500

### 501 **3.3 Mechanical properties**

502 The mechanical properties of neat PVC (PVC-0) and PVC compounds containing 0.1 and  
503 3 wt % ZnPTC-HEMA, prepared with and without ZPT, are summarized in Table 3. The  
504 Young's modulus of PVC-0 ( $10.2 \pm 0.8$  MPa) is not affected by the incorporation of a low  
505 loading of ZnPTC-HEMA (0.1 wt %) nor by the presence of ZPT. In contrast, increasing the  
506 ZnPTC-HEMA content to 3 wt % (PVC-3) leads to a measurable stiffening of the material,  
507 with the modulus rising to  $12.6 \pm 1.7$  MPa in the absence of ZPT and to  $13.0 \pm 1.9$  MPa when  
508 ZPT is present (PVC-3-ZPT). Statistical analysis using a two-sample Student's *t*-test ( $\alpha =$   
509 0.05, 95% confidence level), performed relative to neat PVC, confirms that this increase is  
510 statistically significant only at the highest phthalocyanine loading (3 wt %), irrespective of  
511 ZPT addition. This trend is consistent with the morphological features observed in the SEM  
512 micrographs, which indicate a more rigid microstructure at higher additive contents.

513 The tensile strength (stress at break) of all samples falls within a narrow range of  $7.5 \pm 1.4$  to  
514  $9.9 \pm 1.8$  MPa, while the strain at break varies between  $174.4 \pm 34.8\%$  and  $196.6 \pm 26.2\%$   
515 (Table 3). No statistically significant differences in either tensile strength or elongation at  
516 break are observed compared to neat PVC (PVC-0). These results indicate that, within the  
517 investigated concentration range, ZnPTC-HEMA does not detrimentally affect the ductility or  
518 ultimate strength of the PVC matrix.

519 Pronounced effects of phthalocyanines on polymer mechanical properties have been reported  
520 previously, for example for copper phthalocyanine incorporated into a polyurethane matrix;  
521 however, such effects were observed at substantially higher filler loadings (up to 30 wt %)   
522 (Youssef, Al-Turaif, and Wazzan 2015). In contrast, our findings are in line with reports  
523 describing negligible changes in mechanical performance upon the incorporation of moderate  
524 amounts of photocatalytic additives into PVC, such as 4.8 wt % reported by Yang et al.  
525 (2016). Overall, the present results demonstrate that low to moderate ZnPTC-HEMA loadings  
526 preserve the mechanical integrity of PVC, while higher loadings can induce a modest but  
527 statistically significant increase in stiffness without compromising tensile strength or  
528 elongation.

529

530 **Table 3.** Mechanical Properties of PVC and ZnPTC-HEMA Compounds with/without ZPT  
531 (0.005 wt %)

<b>Samples</b>	<b>Young Modulus (MPa)</b>	<b>Strain at Break (%)</b>	<b>Stress at Break (MPa)</b>
PVC-0	$10.2 \pm 0.8^a$	$185.5 \pm 35.0^a$	$9.7 \pm 1.9^a$
PVC-0.1	$10.8 \pm 0.6^a$	$174.4 \pm 34.8^a$	$8.0 \pm 1.4^a$
PVC- 3	$12.6 \pm 1.7^b$	$196.6 \pm 26.2^a$	$9.9 \pm 1.8^a$
PVC-0-ZPT	$9.7 \pm 0.7^a$	$172.5 \pm 22.4^a$	$9.2 \pm 1.8^a$

PVC-0.1-ZPT	$10.8 \pm 0.1^a$	$196.5 \pm 35.7^a$	$7.5 \pm 1.4^a$
PVC-3-ZPT	$13.0 \pm 1.9^b$	$186.3 \pm 36.3^a$	$9.7 \pm 1.9^a$

532

### 533 3.4 Singlet oxygen quantification

534 The quantitative analysis of singlet oxygen generation, summarized in the Table 3,  
535 demonstrates that incorporation of ZnPTC-HEMA into the PVC matrix markedly enhances  
536 singlet oxygen production relative to neat PVC. The pristine polymer exhibits a very low rate  
537 constant ( $k = 0.0031 \text{ J}^{-1}$ ) and a correspondingly long half-time ( $\tau_{1/2} \approx 5590 \text{ s}$ ), confirming the  
538 negligible intrinsic photosensitizing activity of unmodified PVC under the applied  
539 experimental conditions.

540 Even at the lowest ZnPTC-HEMA loading of 0.1 wt % (PVC-0.1), a pronounced increase in  
541 singlet oxygen generation is observed, with  $k$  increasing by nearly an order of magnitude and  
542  $\tau_{1/2}$  decreasing to approximately 600 s. This sharp transition indicates that ZnPTC-HEMA acts  
543 as a highly efficient photosensitizer within the polymer matrix and that only minimal additive  
544 concentrations are required to activate effective photodynamic behavior. As the ZnPTC-  
545 HEMA content increases from 0.1 to 1 wt % (PVC-1 to PVC-1), a monotonic increase in  $k$  is  
546 accompanied by a progressive reduction in  $\tau_{1/2}$ , reflecting accelerated singlet oxygen  
547 production. The most substantial gains occur up to approximately 0.5–1 wt % (PVC-0.5 to  
548 PVC-1), beyond which further increases in additive content yield only marginal  
549 improvements.

550 At higher loadings (1–3 wt %), the system approaches a plateau regime, with  $k$  values  
551 converging to  $\sim 0.05 \text{ J}^{-1}$  and  $\tau_{1/2}$  stabilizing in the range of 317–333 s. This saturation behavior  
552 suggests that singlet oxygen generation becomes limited by factors other than photosensitizer

553 concentration, such as light absorption efficiency, excited-state quenching, or oxygen  
554 diffusion within the polymer matrix.

555 The addition of ZPT at 0.005 wt % (Table 4) leads to a modest reduction in singlet oxygen  
556 generation across all ZnPTC-HEMA concentrations. This effect is reflected in slightly lower  $k$   
557 values and correspondingly higher  $\tau_{1/2}$  values relative to the ZPT-free systems. Importantly,  
558 the preservation of high singlet oxygen production in the presence of ZPT indicates that the  
559 two antimicrobial strategies, singlet oxygen production and conventional biocidal action, can  
560 coexist without strong antagonistic interactions. This observation is consistent with the  
561 antimicrobial assay results, which show sustained efficacy even in formulations containing  
562 both additives. From an application perspective, these findings support the feasibility of  
563 designing multifunctional PVC materials in which ZnPTC-HEMA provides robust  
564 photodynamic activity at relatively low loadings, while ZPT contributes complementary  
565 antimicrobial protection without significantly impairing ROS generation.

566 All samples were analyzed in triplicate. The relative standard deviation (RSD) for replicate  
567 measurements was below 10% for each sample, demonstrating good repeatability of the  
568 analytical procedure. Accordingly, the measured values were deemed sufficiently reliable for  
569 subsequent evaluation of photoactivity.

570 Overall, the singlet oxygen quantification data highlight an optimal ZnPTC-HEMA  
571 concentration window around 0.5–1 wt %, where high photodynamic efficiency is achieved  
572 without unnecessary additive excess. This balance is particularly relevant for practical  
573 implementation, as it aligns enhanced antimicrobial performance with material stability and  
574 processability requirements expected for advanced polymeric antimicrobial surfaces.

575

576 **Table 4.** Singlet oxygen production as a function of ZnPTC-HEMA concentration  
577 with/without fixed ZPT loading (0.005 wt %)

Sample	ZnPTC-HEMA (wt %)	ZPT (wt %)	$k$ (J <sup>-1</sup> )	$\tau_{1/2}$ (s)
PVC-0	-	-	0.0031	5590
PVC-0.1	0.1	-	0.0287	604
PVC-0.2	0.2	-	0.0373	465
PVC-0.5	0.5	-	0.0492	352
PVC-1	1.0	-	0.0521	333
PVC-3	3.0	-	0.0547	317
PVC-0.1-ZPT	0.1	0.005	0.0272	637
PVC-0.2-ZPT	0.2	0.005	0.0368	471
PVC-0.5-ZPT	0.5	0.005	0.0463	374
PVC-1-ZPT	1.0	0.005	0.0502	345
PVC-3-ZPT	3.0	0.005	0.0452	383

578 All samples were analyzed in triplicate. The relative standard deviation (RSD) for replicate  
579 measurements was below 10% for each sample.

580

### 581 3.5 Antimicrobial assays

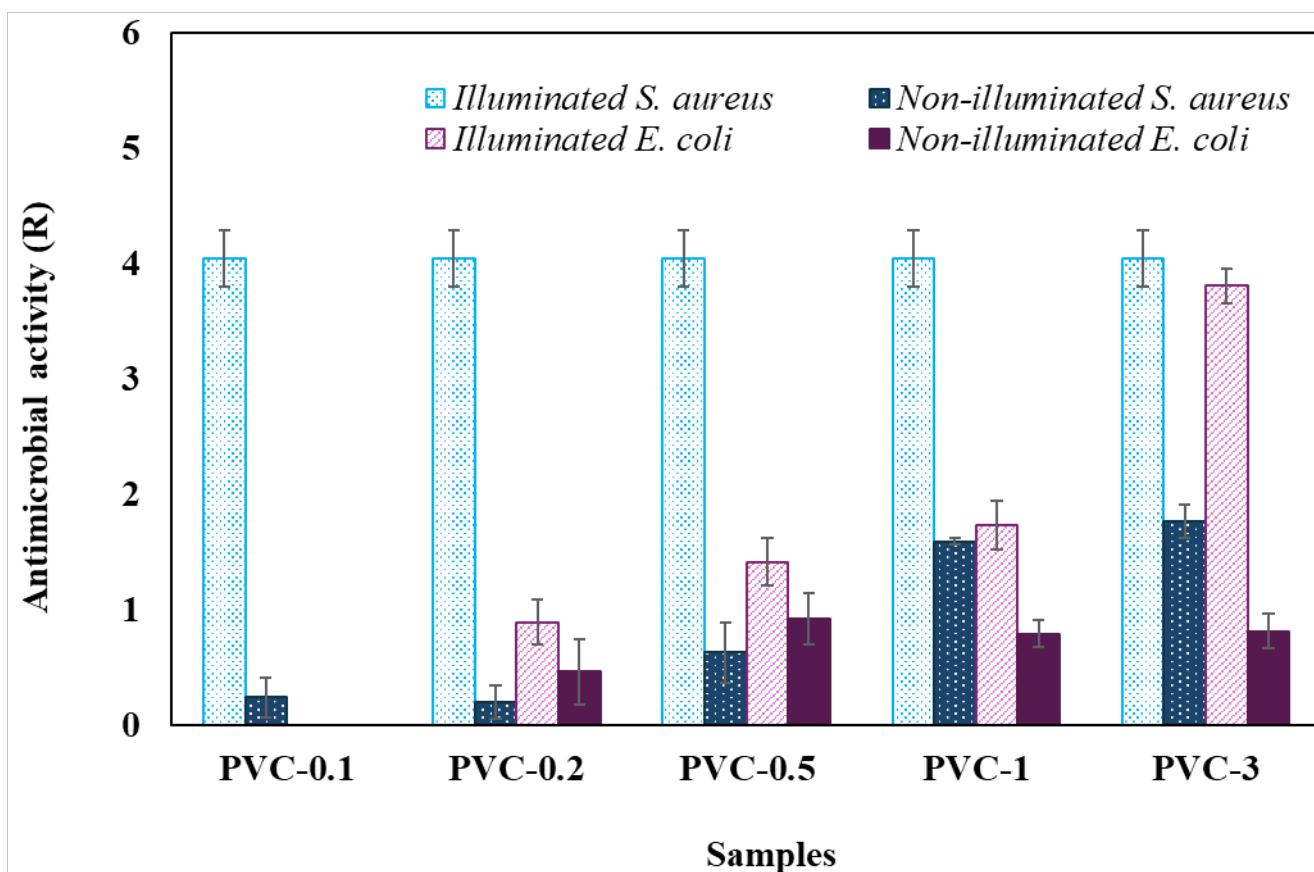
#### 582 Antibacterial efficacy

583 The study results demonstrated that PVC modified with phthalocyanine derivate ZnPTC-  
584 HEMA exhibits pronounced light-activated antimicrobial activity. Under illumination at 1000  
585 lux, the material effectively suppressed the growth of Gram-positive *S. aureus* even at a  
586 loading of 0.1% (PVC-0.1), indicating a bactericidal response (Figure 6). In contrast, Gram-  
587 negative *E. coli* showed substantially lower susceptibility: only weak inhibition was observed  
588 at ZnPTC-HEMA concentrations up to 0.5% ( $R = 1.4 \pm 0.2$ ), while strong antimicrobial

589 activity ( $R = 3.8 \pm 0.1$ ) was achieved only at the highest loading tested (3%) under light  
590 exposure. Samples incubated in the dark exhibited only marginal activity ( $R = 1.6 \pm 0.2$ ),  
591 detectable solely against *S. aureus* at loadings  $\geq 1\%$ , indicating that the effect is primarily  
592 photoactivation-driven rather than due to passive toxicity of the material.

593

594



595

596 **Figure 6.** Antibacterial activity of illuminated/non-illuminated PVC samples with ZnPTC-  
597 HEMA concentration scale against *S. aureus* and *E. coli*.

598

599 The addition of ZPT (0.005 wt %) significantly ( $P > 0.05$ ) enhanced the antimicrobial  
600 properties, even in non-illuminated samples (Figure 7). The figure shows that antimicrobial  
601 efficiency depends on the dye concentration. This enhancement was notable, as strong

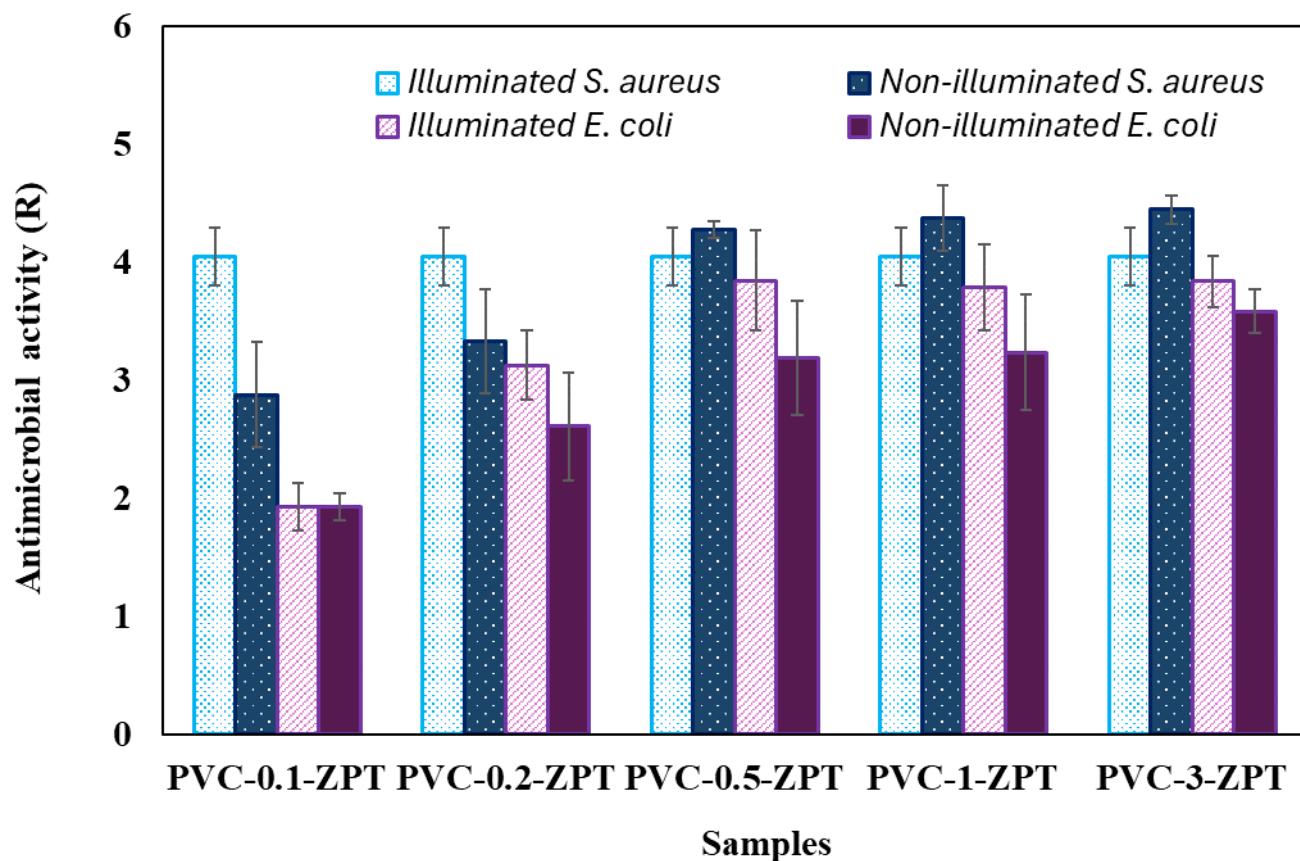
602 antimicrobial activity ( $R > 3$ ) against both monitored bacteria strains at only 0.5% ZnPTC-  
603 HEMA (PVC-0.5-ZPT), suggesting a synergistic enhancement of photodynamic activity.

604

605 The results of the antibacterial activity assessment, summarized in Figures 6 and 7, reveal  
606 higher efficacy against Gram-positive *S. aureus*. This observation aligns with findings  
607 reported in previous studies.<sup>30,46</sup> Grammatikova et al. (2019) demonstrated a strong  
608 antibacterial effect of phthalocyanine-stained paper against *S. aureus* after just 60 minutes of  
609 exposure to light at an intensity of 270 lux.<sup>47</sup> Similarly, Mapukata et al. (2021) also reported  
610 high antibacterial activity against *S. aureus* under illumination.<sup>48</sup>

611 The photodynamic mechanism of phthalocyanines is well established and involves light  
612 absorption followed by intersystem crossing to the triplet excited state and subsequent  
613 electron energy transfer to molecular oxygen. This process generates reactive oxygen species,  
614 including singlet oxygen, which exhibit potent antibacterial effects.<sup>48</sup> Some studies have  
615 shown that these species can penetrate the porous peptidoglycan layer of Gram-positive  
616 bacteria, making them more susceptible to photodynamic inactivation.<sup>49-51</sup>

617 In contrast, Gram-negative bacteria possess an additional outer lipopolysaccharide layer,  
618 which reduces their permeability to lipophilic small molecules and increases their resistance  
619 to both antibiotics and photodynamic treatments. However, the photosensitivity of Gram-  
620 negative bacteria can be enhanced by substances such as  $\text{CaCl}_2$ , EDTA, or polymyxin B,  
621 which alter outer membrane permeability. The underlying reasons for Gram-negative  
622 bacteria's resistance to photosensitization remain unclear but may involve the charge on the  
623 photosensitizer and its resulting subcellular distribution and localization within these  
624 organisms.<sup>49,50</sup> Additionally, weak antimicrobial activity against *E. coli* was also recently  
625 demonstrated for a polyhydroxybutyrate submicron fiber mat with 0.1 wt % zinc  
626 phthalocyanine derivative content.<sup>51</sup>



627

628 **Figure 7.** Antibacterial activity of illuminated/non-illuminated PVC samples with ZnPTC-  
 629 HEMA concentration scale and ZPT (0.005 wt %) against *S. aureus* and *E. coli*.

630

### 631 Antiviral efficacy

632 The antibacterial activity of the prepared samples was assessed following the ISO 22196:2021  
 633 standard, with protocol modifications to accommodate bacteriophage propagation  
 634 requirements. Table 5 summarizes the antiviral performance of illuminated and non-  
 635 illuminated PVC specimens incorporating increasing concentrations of ZnPTC-HEMA.  
 636 Antiviral efficacy was assessed against the enveloped bacteriophage  $\Phi 6$  and the non-  
 637 enveloped bacteriophage  $\Phi X174$ .

638 The results demonstrate that incorporation of 0.1 wt % ZnPTC-HEMA yields (PVC-0.1) a  
 639 statistically significant ( $P < 0.05$ ) microbicidal effect against  $\Phi 6$  under light irradiation ( $R =$   
 640  $5.1 \pm 0.2$ ). In contrast, no measurable antiviral activity was detected in samples maintained

63  
 64

641 under dark conditions. Furthermore, no reduction in infectivity was observed for  $\Phi$ X174  
 642 under either illuminated or non-illuminated conditions, indicating that singlet oxygen  
 643 generated upon irradiation selectively inactivates the enveloped bacteriophage  $\Phi$ 6 but does  
 644 not affect the non-enveloped  $\Phi$ X174.

645

646 **Table 5.** Antiviral activity of illuminated/non-illuminated PVC samples with ZnPTC-HEMA  
 647 concentration scale

Sample →		PVC-0.1	PVC-0.2	PVC-1	PVC-3
Phage ↓	ZnPTC-HEMA (wt %) →	0.1	0.2	1	3
	<b>R <math>\Phi</math>6</b>	Illuminated	5.1±0.2	5.1±0.2	5.1±0.2
Non-illuminated		0±0.0	0.1±0.0	0±0.0	0±0.0
<b>R <math>\Phi</math>X174</b>	Illuminated	-	-	-	0.2±0.02
	Non-illuminated	-	-	-	0±0.0

648 The antiviral test results in Table 6 indicate, in contrast to the tested bacteria, that the addition  
 649 of ZPT did not improve the antiviral efficacy of the samples against either tested  
 650 bacteriophage.

651

652 **Table 6.** Antiviral activity of illuminated/non-illuminated PVC samples with ZnPTC-HEMA  
 653 concentration scale and ZPT (0.005 wt %)

Sample →		PVC-0.1-ZPT	PVC-0.2-ZPT	PVC-1-ZPT	PVC-3-ZPT
Phage ↓	ZnPTC-HEMA (wt %) →	0.1	0.2	1	3

<b>R Φ6</b>	Illuminated	5.2±0.2	5.2±0.2	5.2±0.2	5.2±0.2
	Non-illuminated	0±0.0	0.1±0.0	0±0.0	0±0.0
<b>R ΦX174</b>	Illuminated	-	-	-	0.5±0.1
	Non-illuminated	-	-	-	0.4±0.1

654 The pronounced antiviral efficacy of singlet oxygen against bacteriophage Φ6 was expected,  
655 as its effectiveness against enveloped viruses has been documented in several studies.<sup>52,53</sup>  
656 Efimov et al. (2024) reported a 99.97% (3.4 log) reduction in the viral load of enveloped  
657 SARS-CoV 227 upon light exposure of fabrics functionalized with the tetracationic zinc  
658 phthalocyanine derivative LASU.<sup>14</sup>

659 Singlet oxygen is highly active and readily reacts with diverse biological macromolecules,  
660 including nucleic acids, proteins, and lipids. In DNA, it preferentially oxidizes guanine  
661 residues and can induce covalent cross-links between guanine and lysine.<sup>25</sup> In enveloped  
662 viruses, singlet oxygen also targets the lipid components of the viral envelope, a phospholipid  
663 bilayer embedded with membrane proteins and receptor-binding glycoproteins, leading to  
664 oxidative damage that compromises viral integrity and infectivity.<sup>52,54</sup>

665 Pyrithione has been shown to inhibit infection by human rhinovirus, coxsackievirus, and  
666 mengovirus, RNA viruses belonging to the Picornaviridae family. Additionally, Qiu et al.  
667 (2013) reported that pyrithione exhibits inhibitory activity against HSV-1 and HSV-2 at non-  
668 cytotoxic concentrations. These viruses, members of the Herpesviridae family, are large DNA  
669 viruses.<sup>55</sup> Although phage Φ6, a member of the *Cystoviridae* family, has been successfully  
670 used as a surrogate for enveloped viruses, incorporation of 50 mg of ZPT to PVC did not  
671 produce measurable antiviral activity. This concentration was selected in accordance with the  
672 manufacturer's recommendation (Alchimica CZ), but it appears to be insufficient to elicit an  
673 antiviral effect under the conditions tested. Moreover, in contrast to the bacterial assays, no

674 synergistic interaction was observed. Increasing the zinc pyrithione content to 0.01 wt %  
675 likewise failed to enhance antiviral efficacy.

676

677 Phage  $\Phi$ X174 is one of the most resilient non-enveloped viruses, with an outer wall  
678 composed of a robust protein coat that withstands most disinfectants.<sup>56</sup> Our findings show that  
679 it resisted even the highest tested concentration of ZnPTC-HEMA in the PVC matrix at 3 wt  
680 % and the addition of ZPT (0.005 wt %).

681

### 682 **3.6 Migration study evaluation**

683 The objective of this study was to assess whether ZnPTC-HEMA migrates from PVC into an  
684 aqueous environment and, if so, to quantify its concentration. After 10 days of exposure  
685 (40 °C, distilled water), ZnPTC-HEMA was not detected in any of the eluates ( $c < \text{LOD}$ ) by  
686 UV-Vis analysis and EDX method. These findings suggest strong retention of ZnPTC-HEMA  
687 within the PVC matrix, likely attributable to its high molecular weight and low aqueous  
688 solubility.

689

### 690 **3.7. Limitations and future directions**

691 Despite the promising performance demonstrated herein, several limitations should be  
692 acknowledged. Antiviral efficacy was evaluated using bacteriophage surrogates under  
693 controlled laboratory conditions; although  $\Phi$ 6 and  $\Phi$ X174 are well-established models,  
694 confirmation against clinically relevant human viruses is necessary to fully establish  
695 translational relevance. In addition, long-term photostability, durability under repeated  
696 cleaning or mechanical abrasion, and performance in complex biological matrices were not  
697 assessed. Future work should therefore address real-world aging behavior, biofilm formation  
698 under continuous use, cytocompatibility and regulatory safety considerations, and

699 optimization of photosensitizer architecture to enhance activity against Gram-negative  
700 bacteria and non-enveloped viruses. Such investigations will be essential for advancing this  
701 platform toward practical medical and high-touch surface applications.

702

### 703 **Conclusion**

704 This study shows that incorporation of a methacrylate-functionalized zinc phthalocyanine  
705 (ZnPTC-HEMA) into PVC provides efficient, light-activated antimicrobial functionality at  
706 remarkably low additive loadings. Singlet oxygen generation increased sharply at 0.1 wt %  
707 and approached a plateau above approximately 1 wt %, identifying a practical composition  
708 window that balances photoactivity, processability, of material properties. Under visible light,  
709 the materials achieved complete photoinactivation (>5 log reduction) of the enveloped  
710 bacteriophage  $\Phi 6$ , while the structurally robust non-enveloped  $\Phi X174$  remained unaffected,  
711 underscoring the key role of lipid envelope oxidation in the antiviral mechanism.

712 The materials also exhibited pronounced photodynamic antibacterial activity, particularly  
713 against *S. aureus*, while *E. coli* required higher photosensitizer loadings, consistent with the  
714 greater permeability barrier of Gram-negative cell envelopes. Incorporation of ZPT  
715 at 0.005 wt % provided complementary dark-active antibacterial protection and broadened the  
716 antimicrobial profile without substantially reducing reactive oxygen species generation.

717 Materials characterization further confirmed good compatibility of the antimicrobial additives  
718 with the PVC matrix across the practically relevant concentration range. Noticeable structural  
719 disruption was observed only at the highest loading tested (3 wt % ZnPTC-HEMA), in  
720 agreement with the mechanical data. Statistically significant deterioration in mechanical  
721 performance was likewise detected only at this concentration, indicating that lower additive  
722 contents preserve the structural and functional integrity of the PVC foils. FTIR analysis  
723 showed that even the highest concentrations of ZnPTC-HEMA and ZPT did not measurably

71  
72

724 alter the chemical environment of the PVC chains. In addition, migration experiments  
725 revealed negligible additive release, supporting the stability of the material system during  
726 prolonged aqueous exposure.

727 Overall, the combination of strong photodynamic antiviral activity against an enveloped virus  
728 surrogate, enhanced antibacterial performance, retained mechanical integrity at low additive  
729 content, and minimal additive migration establishes ZnPTC-HEMA-modified PVC as a  
730 promising platform for antimicrobial surfaces and medical-material surfaces. More broadly,  
731 these findings demonstrate the feasibility of integrating photoactive phthalocyanines into  
732 melt-processable PVC formulations to produce multifunctional materials for passive and  
733 light-triggered disinfection.

734

#### 735 **Notes**

736 The authors declare no competing financial interest.

#### 737 **ACKNOWLEDGMENTS**

738 This work was supported from the European Just Transition Fund within the Operational  
739 Programme: Just Transition under the aegis of the Ministry of the Environment of the Czech  
740 Republic, project Operational Programme Johannes Amos Comenius OP JAC "Application  
741 potential development in the field of polymer materials in the context of circular economy  
742 compliance (POCEK)", number CZ.02.01.01/00/23\_021/0009004.

743 Authors are further grateful for co-funding from the development process of Centre of  
744 Polymer Systems, Tomas Bata University in Zlin, program DKRVO (RP/CPS/2024-28/002)  
745 supported by the Ministry of Education Youth and Sports of the Czech Republic.

746

747 **Acknowledgments**

748 Data will be made available on request.

749

750 **References**

~~751~~ Dunning, J.; Thwaites, R. S.; Openshaw, P. J. M. Seasonal and Pandemic Influenza: 100 Years

752 of Progress, Still Much to Learn. *Mucosal Immunol.* 2020, 13 (4), 566–573.

753 <https://doi.org/10.1038/s41385-020-0287-5>.

~~754~~ Harrington, W. N.; Kackos, C. M.; Webby, R. J. The Evolution and Future of Influenza

755 Pandemic Preparedness. *Exp. Mol. Med.* 2021, 53 (5), 737–749.

756 <https://doi.org/10.1038/s12276-021-00603-0>.

~~757~~ Morens, D. M.; Taubenberger, J. K.; Fauci, A. S. Predominant Role of Bacterial Pneumonia as

758 a Cause of Death in Pandemic Influenza: Implications for Pandemic Influenza Preparedness.

759 *J. Infect. Dis.* 2008, 198 (7), 962–970. <https://doi.org/10.1086/591708>.

~~760~~ Ordon, M.; Nawrotek, P.; Stachurska, X.; Mizielińska, M. Polyethylene Films Coated with

761 Antibacterial and Antiviral Layers Based on CO<sub>2</sub> Extracts of Raspberry Seeds, of

762 Pomegranate Seeds and of Rosemary. *Coatings 2021, Vol. 11, Page 1179* 2021, 11 (10), 1179.

763 <https://doi.org/10.3390/COATINGS11101179>.

~~764~~ Olewnik-Kruszkowska, E.; Gierszewska, M.; Jakubowska, E.; Tarach, I.; Sedlarik, V.;

765 Pummerova, M. Antibacterial Films Based on PVA and PVA–Chitosan Modified with

766 Poly(Hexamethylene Guanidine). *Polymers (Basel)*. 2019, 11 (12), 2093.

767 <https://doi.org/10.3390/polym11122093>.

- 768 Donnadio, A.; Roscini, L.; Di Michele, A.; Corazzini, V.; Cardinali, G.; Ambrogi, V. PVC  
769 Grafted Zinc Oxide Nanoparticles as an Inhospitable Surface to Microbes. *Materials Science  
770 and Engineering: C* 2021, 128, 112290. <https://doi.org/10.1016/j.msec.2021.112290>.
- 771 Elgharbawy, A. Poly Vinyl Chloride Additives and Applications-A Review. *Journal of Risk  
772 Analysis and Crisis Response* 2022, 12 (3). <https://doi.org/10.54560/jracr.v12i3.335>.
- 783 Trousil, V.; Černý, J.; Kořínková, R.; Pummerová, M.; Mikulcová, V.; Herynková, M.  
774 Degradation of a Model Dye with Zinc Phthalocyanine Sulphonamide Embedded in Polymer  
775 Matrices. *J. Photochem. Photobiol. A Chem.* 2021, 405, 112985.  
776 <https://doi.org/10.1016/j.jphotochem.2020.112985>.
- 797 María Curieses Andrés, C.; Manuel Pérez de la Lastra, J.; Andrés Juan, C.; J. Plou, F.; Pérez-  
778 Lebeña, E. Reactivity and Applications of Singlet Oxygen Molecule; 2024.  
779 <https://doi.org/10.5772/intechopen.112024>.
- 780 Dharmaratne, P.; Wang, B.; Wong, R. C. H.; Chan, B. C. L.; Lau, K.-M.; Ke, M.-R.; Lau, C.  
781 B. S.; Ng, D. K. P.; Fung, K.-P.; Ip, M. Monosubstituted Tricationic Zn(II) Phthalocyanine  
782 Enhances Antimicrobial Photodynamic Inactivation (APDI) of Methicillin-Resistant  
783 *Staphylococcus Aureus* (MRSA) and Cytotoxicity Evaluation for Topical Applications: *In  
784 Vitro* and *in Vivo* Study. *Emerg. Microbes Infect.* 2020, 9 (1), 1628–1637.  
785 <https://doi.org/10.1080/22221751.2020.1790305>.
- 786 de Siqueira, L. B. de O.; dos Santos Matos, A. P.; da Silva, M. R. M.; Pinto, S. R.; Santos-  
787 Oliveira, R.; Ricci-Júnior, E. Pharmaceutical Nanotechnology Applied to Phthalocyanines for  
788 the Promotion of Antimicrobial Photodynamic Therapy: A Literature Review. *Photodiagnosis  
789 Photodyn. Ther.* 2022, 39, 102896. <https://doi.org/10.1016/j.pdpdt.2022.102896>.

- 790 Galstyan, A. Turning Photons into Drugs: Phthalocyanine-Based Photosensitizers as Efficient  
791 Photoantimicrobials. *Chemistry – A European Journal* 2021, 27 (6), 1903–1920.  
792 <https://doi.org/10.1002/chem.202002703>.
- 793 Grammatikova, N. E.; George, L.; Ahmed, Z.; Candeias, N. R.; Durandin, N. A.; Efimov, A.  
794 Zinc Phthalocyanine Activated by Conventional Indoor Light Makes a Highly Efficient  
795 Antimicrobial Material from Regular Cellulose. *J. Mater. Chem. B* 2019, 7 (28), 4379–4384.  
796 <https://doi.org/10.1039/C9TB01095E>.
- 797 Efimov, A.; Dagallier, C.; Frochot, C.; Myrzakhmetov, B.; Arnoux, P.; Heinonen, T.;  
798 Mannerström, M.; Toimela, T.; Ahmed, Z.; Audibert, J. F.; Habermeyer, B.; Mordon, S.;  
799 Pansu, R. B. LASU: An Efficient and Stable Phthalocyanine Dye with Tolerable Safety  
800 Profile for Self-Disinfecting Anti-COVID Textiles Activated by Ambient Light.  
801 *Photodiagnosis Photodyn. Ther.* 2024, 45, 103978.  
802 <https://doi.org/10.1016/j.pdpdt.2024.103978>.
- 803 Fang, R.; Xu, W.; Yuan, C.; Sun, D.; Guo, Y.; Xu, Y. Light-Activated Antibacterial Zinc  
804 Phthalocyanine–Polycaprolactone/Gelatin Hybrid Fibrous Membranes for Wound Healing.  
805 *ACS Applied Engineering Materials* 2026, 4 (2), 1093–1104.  
806 <https://doi.org/10.1021/acsaenm.5c01164>.
- 807 Marin, M. L.; Santos-Juanes, L.; Arques, A.; Amat, A. M.; Miranda, M. A. Organic  
808 Photocatalysts for the Oxidation of Pollutants and Model Compounds. *Chem. Rev.* 2012, 112  
809 (3), 1710–1750. <https://doi.org/10.1021/cr2000543>.
- 810 Vyskocil, J. M.; Turgeon, N.; Turgeon, J. G.; Duchaine, C. Ozone Treatment in a Wind Tunnel  
811 for the Reduction of Airborne Viruses in Swine Buildings. *Aerosol Science and Technology*  
812 2020, 1471–1478. <https://doi.org/10.1080/02786826.2020.1790495>.

- 818) Turgeon, N.; Toulouse, M. J.; Martel, B.; Moineau, S.; Duchaine, C. Comparison of Five  
814 Bacteriophages as Models for Viral Aerosol Studies. *Appl. Environ. Microbiol.* 2014, *80* (14),  
815 4242–4250. <https://doi.org/10.1128/AEM.00767-14>.
- 816) Serrano-Aroca, Á. Antiviral Characterization of Advanced Materials: Use of Bacteriophage  
817 Phi 6 as Surrogate of Enveloped Viruses Such as SARS-CoV-2. *International Journal of*  
818 *Molecular Sciences*. MDPI May 1, 2022. <https://doi.org/10.3390/ijms23105335>.
- 819) Franke, G.; Knobling, B.; Brill, F. H.; Becker, B.; Klupp, E. M.; Belmar Campos, C.;  
820 Pfefferle, S.; Lütgehetmann, M.; Knobloch, J. K. An Automated Room Disinfection System  
821 Using Ozone Is Highly Active against Surrogates for SARS-CoV-2. *Journal of Hospital*  
822 *Infection* 2021, *112*, 108–113. <https://doi.org/10.1016/j.jhin.2021.04.007>.
- 823) Fedorenko, A.; Grinberg, M.; Orevi, T.; Kashtan, N. Survival of the Enveloped Bacteriophage  
824 Phi6 (a Surrogate for SARS-CoV-2) in Evaporated Saliva Microdroplets Deposited on Glass  
825 Surfaces. *Sci. Rep.* 2020, *10* (1), 22419. <https://doi.org/10.1038/s41598-020-79625-z>.
- 826) Dey, R.; Dlusskaya, E.; Ashbolt, N. J. SARS-CoV-2 Surrogate ( Phi6 ) Environmental  
827 Persistence within Free-Living Amoebae . *J. Water Health* 2021.  
828 <https://doi.org/10.2166/WH.2021.167>.
- 829) Lytle, C. D.; Truscott, W.; Budacz, A. P.; Venegas, L.; Routson, L. B.; Cyr, W. H. Important  
830 Factors for Testing Barrier Materials with Surrogate Viruses. *Appl. Environ. Microbiol.* 1991,  
831 *57* (9), 2549–2554. <https://doi.org/10.1128/aem.57.9.2549-2554.1991>.
- 832) Heffron, J.; Samsami, M.; Juedemann, S.; Lavin, J.; Tavakoli Nick, S.; Kieke, B. A.; Mayer,  
833 B. K. Mitigation of Viruses of Concern and Bacteriophage Surrogates via Common Unit  
834 Processes for Water Reuse: A Meta-Analysis. *Water Res.* 2024, *252*, 121242.  
835 <https://doi.org/10.1016/j.watres.2024.121242>.

- 836 Guo, L.; Xu, R.; Gou, L.; Liu, Z.; Zhao, Y.; Liu, D.; Zhang, L.; Chen, H.; Kong, M. G.  
837 Mechanism of Virus Inactivation by Cold Atmospheric-Pressure Plasma and Plasma-  
838 Activated Water. *Appl. Environ. Microbiol.* 2018, 84 (17).  
839 <https://doi.org/10.1128/AEM.00726-18>.
- 840 Pop, F.; Humphreys, J.; Schwarz, J.; Brown, L.; van den Berg, A.; Amabilino, D. B. Towards  
841 More Sustainable Synthesis of Diketopyrrolopyrroles. *New Journal of Chemistry* 2019, 43  
842 (15), 5783–5790. <https://doi.org/10.1039/C9NJ01074B>.
- 843 Beran, M.; Horna, A.; Vorisek, V.; Berkova, E.; Korinkova, R.; Trousil, V.; Hrubanova, M.  
844 Antimicrobial Polyhydroxybutyrate Submicron Fiber Mat Loaded with Extract of *Hypericum*  
845 *Perforatum*. *J. Plant Biotechnol.* 2022, 49 (3), 257–270.  
846 <https://doi.org/10.5010/JPB.2022.49.3.257>.
- 847 Bazant, P.; Kuritka, I.; Hudecek, O.; Machovsky, M.; Mrlik, M.; Sedlacek, T. Microwave-  
848 assisted Synthesis of Ag/ZnO Hybrid Filler, Preparation, and Characterization of Antibacterial  
849 Poly(Vinyl Chloride) Composites Made from the Same. *Polym. Compos.* 2014, 35 (1), 19–26.  
850 <https://doi.org/10.1002/pc.22629>.
- 851 Essawy, H. A.; Abd El-Wahab, N. A.; Abd El-Ghaffar, M. A. PVC–Laponite Nanocomposites:  
852 Enhanced Resistance to UV Radiation. *Polym. Degrad. Stab.* 2008, 93 (8), 1472–1478.  
853 <https://doi.org/10.1016/j.polymdegradstab.2008.05.015>.
- 854 Trousil, V.; Černý, J.; Kořínková, R.; Pummerová, M.; Mikulcová, V.; Herynková, M.  
855 Degradation of a Model Dye with Zinc Phthalocyanine Sulphonamide Embedded in Polymer  
856 Matrices. *J. Photochem. Photobiol. A Chem.* 2021, 405, 112985.  
857 <https://doi.org/10.1016/j.jphotochem.2020.112985>.
- 858 Colthup, N. B. ; Daly, L. H. .; Wiberley, S. E. . *Introduction to Infrared and Raman*  
859 *Spectroscopy*; Academic Press, 1990.

- 860) Smith, B. C. *Fundamentals of Fourier Transform Infrared Spectroscopy*; CRC Press, 2011.  
861 <https://doi.org/10.1201/b10777>.
- 862) Pittol, M.; Tomacheski, D.; Simões, D. N.; Ribeiro, V. F.; Santana, R. M. C. Antimicrobial  
863 Performance of Thermoplastic Elastomers Containing Zinc Pyrithione and Silver  
864 Nanoparticles. *Materials Research* 2017, 20 (5), 1266–1273. [https://doi.org/10.1590/1980-](https://doi.org/10.1590/1980-5373-mr-2017-0137)  
865 5373-mr-2017-0137.
- 866) Deleanu, I. M.; Grosu, E.; Ficai, A.; Ditu, L. M.; Motelica, L.; Oprea, O.-C.; Gradisteanu  
867 Pircalabioru, G.; Sonmez, M.; Busuioc, C.; Ciocoiu, R.; Antoniac, V. I. New Antimicrobial  
868 Materials Based on Plasticized Polyvinyl Chloride for Urinary Catheters: Preparation and  
869 Testing. *Polymers (Basel)*. 2024, 16 (21), 3028. <https://doi.org/10.3390/polym16213028>.
- 870) Rouabah, N.; Nazir, R.; Djaballah, Y.; Mir, A. Q.; Ameer, I.; Beldjebli, O. Synthesis of a Thin  
871 Film of CuO/MgO/PVC Nanocomposites for Photocatalytic Applications. *Iranian Journal of*  
872 *Catalysis* 2023, 13 (1), 23–34. <https://doi.org/10.30495/IJC.2023.1970800.1968>.
- 873) Nel, H. A.; Chetwynd, A. J.; Kelly, C. A.; Stark, C.; Valsami-Jones, E.; Krause, S.; Lynch, I.  
874 An Untargeted Thermogravimetric Analysis-Fourier Transform Infrared-Gas  
875 Chromatography-Mass Spectrometry Approach for Plastic Polymer Identification. *Environ.*  
876 *Sci. Technol.* 2021, 55 (13), 8721–8729. <https://doi.org/10.1021/acs.est.1c01085>.
- 877) Altarawneh, S.; Al-Harashsheh, M.; Dodds, C.; Buttress, A.; Kingman, S. Thermal  
878 Degradation Kinetics of Polyvinyl Chloride in Presence of Zinc Oxide. *Thermochim. Acta*  
879 2022, 707, 179105. <https://doi.org/10.1016/j.tca.2021.179105>.
- 880) Sin, M. C.; Tan, I. K. P.; Annuar, M. S. M.; Gan, S. N. Thermal Behaviour and  
881 Thermodegradation Kinetics of Poly(Vinyl Chloride) Plasticized with Polymeric and  
882 Oligomeric Medium-Chain-Length Poly(3-Hydroxyalkanoates). *Polym. Degrad. Stab.* 2012,  
883 97 (11), 2118–2127. <https://doi.org/10.1016/j.polymdegradstab.2012.08.020>.

- ~~884~~ Rijavec, T. Plastics in Heritage Collections: Poly(Vinyl Chloride) Degradation and  
885 Characterization. *Acta Chim. Slov.* 2020, 67 (4), 993–1013.  
886 <https://doi.org/10.17344/acsi.2020.6479>.
- ~~887~~ Bouchoul, B.; Benaniba, M. T.; Massardier, V. Effect of Biobased Plasticizers on Thermal,  
888 Mechanical, and Permanence Properties of Poly(Vinyl Chloride). *Journal of Vinyl and*  
889 *Additive Technology* 2014, 20 (4), 260–267. <https://doi.org/10.1002/vnl.21356>.
- ~~890~~ Das, S.; Khubdikar, K. A Simple and Facile Spectrophotometric Tool for Quantification of  
891 Zinc Pyrithione (ZPT) in Suspension. *Chemical Data Collections* 2019, 19, 100175.  
892 <https://doi.org/10.1016/j.cdc.2018.100175>.
- ~~893~~ Mesquita, P. J. P. de; Braz, C. J. de F.; Alves, T. S.; Barbosa, R. Bio-High Density  
894 Polyethylene Films Embedded with Organoclay and Zinc Pyrithione. *Polímeros* 2024, 34 (1).  
895 <https://doi.org/10.1590/0104-1428.20230100>.
- ~~896~~ McCann, K.; Knudsen, B.; Ananthoji, R.; Perry, J. J.; Hilker, B.; Zaworotko, M. J.; Harmon,  
897 J. P. Study of Polymeric Interactions of Copolymers: 2-Hydroxyethyl Methacrylate (HEMA)  
898 and 2,3-Dihydroxypropyl Methacrylate (DHPMA) with Copper Hydroxylated Nanoballs. *J.*  
899 *Nanosci. Nanotechnol.* 2010, 10 (9), 5557–5569. <https://doi.org/10.1166/jnn.2010.2498>.
- ~~900~~ Guo, B.; He, Y.; Chen, Y.; Yang, T.; Peng, C.; Luo, W.; Zeng, B.; Xu, Y.; Dai, L. Layered  
901 Double Hydroxide Nanosheets Incorporated Hierarchical Hydrogen Bonding Polymer  
902 Networks for Transparent and Fire-Proof Ceramizable Coatings. *Nanomicro Lett.* 2025, 17  
903 (1), 116. <https://doi.org/10.1007/s40820-025-01646-y>.
- ~~904~~ Mutlu, F.; Pişkin, M.; Canpolat, E.; Öztürk, Ö. F. The New Zinc(II) Phthalocyanine Directly  
905 Conjugated with 4-Butylmorpholine Units: Synthesis, Characterization, Thermal,  
906 Spectroscopic and Photophysical Properties. *J. Mol. Struct.* 2020, 1201, 127169.  
907 <https://doi.org/10.1016/j.molstruc.2019.127169>.

- 906) de Siqueira, L. B. de O.; dos Santos Matos, A. P.; da Silva, M. R. M.; Pinto, S. R.; Santos-  
909 Oliveira, R.; Ricci-Júnior, E. Pharmaceutical Nanotechnology Applied to Phthalocyanines for  
910 the Promotion of Antimicrobial Photodynamic Therapy: A Literature Review. *Photodiagnosis*  
911 *Photodyn. Ther.* 2022, 39, 102896. <https://doi.org/10.1016/j.pdpdt.2022.102896>.
- 912) Grammatikova, N. E.; George, L.; Ahmed, Z.; Candeias, N. R.; Durandin, N. A.; Efimov, A.  
913 Zinc Phthalocyanine Activated by Conventional Indoor Light Makes a Highly Efficient  
914 Antimicrobial Material from Regular Cellulose. *J. Mater. Chem. B* 2019, 7 (28), 4379–4384.  
915 <https://doi.org/10.1039/C9TB01095E>.
- 916) Mapukata, S.; Britton, J.; Osifeko, O. L.; Nyokong, T. The Improved Antibacterial Efficiency  
917 of a Zinc Phthalocyanine When Embedded on Silver Nanoparticle Modified Silica  
918 Nanofibers. *Photodiagnosis Photodyn. Ther.* 2021, 33, 102100.  
919 <https://doi.org/10.1016/j.pdpdt.2020.102100>.
- 920) Sperandio, F.; Huang, Y.-Y.; Hamblin, M. Antimicrobial Photodynamic Therapy to Kill Gram-  
921 Negative Bacteria. *Recent Pat. Antiinfect. Drug Discov.* 2013, 8 (2), 108–120.  
922 <https://doi.org/10.2174/1574891X113089990012>.
- 923) Minnock, A.; Vernon, D. I.; Schofield, J.; Griffiths, J.; Howard Parish, J.; Brown, S. B.  
924 Photoinactivation of Bacteria. Use of a Cationic Water-Soluble Zinc Phthalocyanine to  
925 Photoinactivate Both Gram-Negative and Gram-Positive Bacteria. *J. Photochem. Photobiol. B*  
926 1996, 32 (3), 159–164. [https://doi.org/10.1016/1011-1344\(95\)07148-2](https://doi.org/10.1016/1011-1344(95)07148-2).
- 927) Beran, M.; Korinkova, R.; Polaskova, H.; Drahorad, J.; Vltavsky, O. Antimicrobial  
928 Polyhydroxybutyrate Submicron Fiber Mat Loaded with Zinc Phthalocyanine Derivative.  
929 *Journal of Scientific and Engineering Research*, 2019, 6 (2), 44–56.
- 930) Zeng, L.; Wang, M.-D.; Ming, S.-L.; Li, G.-L.; Yu, P.-W.; Qi, Y.-L.; Jiang, D.-W.; Yang, G.-Y.;  
931 Wang, J.; Chu, B.-B. An Effective Inactivant Based on Singlet Oxygen-Mediated Lipid

- 932 Oxidation Implicates a New Paradigm for Broad-Spectrum Antivirals. *Redox Biol.* 2020, 36,  
933 101601. <https://doi.org/10.1016/j.redox.2020.101601>.
- ~~934~~ Schneider, J. E.; Tabatabaie, T.; Mardt, L.; Smith, R. H.; Nguyen, X.; Pye, Q.; Floyd, R. A.  
935 Potential Mechanisms of Photodynamic Inactivation of Virus by Methylene Blue I. RNA-  
936 Protein Crosslinks and Other Oxidative Lesions in Qbeta Bacteriophage. *Photochem.*  
937 *Photobiol.* 1998, 67 (3), 350–357. <https://doi.org/10.1111/j.1751-1097.1998.tb05209.x>.
- ~~938~~ Serrano-Aroca, Á. Antiviral Characterization of Advanced Materials: Use of Bacteriophage  
939 Phi 6 as Surrogate of Enveloped Viruses Such as SARS-CoV-2. *Int. J. Mol. Sci.* 2022, 23 (10),  
940 5335. <https://doi.org/10.3390/ijms23105335>.
- ~~941~~ Qiu, M.; Chen, Y.; Chu, Y.; Song, S.; Yang, N.; Gao, J.; Wu, Z. Zinc Ionophores Pyrithione  
942 Inhibits Herpes Simplex Virus Replication through Interfering with Proteasome Function and  
943 NF-KB Activation. *Antiviral Res.* 2013, 100 (1), 44–53.  
944 <https://doi.org/10.1016/j.antiviral.2013.07.001>.
- ~~945~~ Cheng, R.; Zhang, Y.; Zhang, T.; Hou, F.; Cao, X.; Shi, L.; Jiang, P.; Zheng, X.; Wang, J. The  
946 Inactivation of Bacteriophages MS2 and PhiX174 by Nanoscale Zero-Valent Iron: Resistance  
947 Difference and Mechanisms. *Frontiers of Environmental Science & Engineering* 2022 16:8  
948 2022, 16 (8), 1–10. <https://doi.org/10.1007/S11783-022-1529-4>.
- 949